Energy & Buildings 317 (2024) 114403

Contents lists available at ScienceDirect

Energy & Buildings

journal homepage: www.elsevier.com/locate/enb

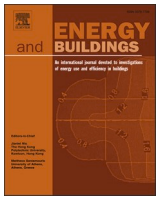

Weather ageing effects on the long-term thermal conductivity and biological colonisation of thermal insulating mortars with EPS, cork and aerogel

Léo Pinchard [a,b], João L. Parracha [a,c,*], Rosário Veiga [a], Luís Matias [a], António Santos Silva [a], Sónia Duarte [a], Lina Nunes [a,d]

[a] LNEC, National Laboratory for Civil Engineering, Av. do Brasil, 101, 1700-066 Lisbon, Portugal
[b] École Centrale de Lyon, 36 Avenue Guy de Collongue, 69134 Ecully Cedex, France
[c] CERIS, DECivil, Instituto Superior Técnico, University of Lisbon, Av. Rovisco Pais, 1040-001 Lisbon, Portugal
[d] cE3c, Centre for Ecology, Evolution and Environmental Changes & CHANGE, Global Change and Sustainability Institute, Azorean Biodiversity Group, University of Azores, 9700-042 Angra do Heroísmo, Azores, Portugal

ARTICLE INFO

Keywords:
Thermal insulation materials
Thermal mortars
Durability assessment
Accelerated ageing
Thermal performance
Mould growth

ABSTRACT

The use of thermal insulation materials in the opaque walls is one of the best strategies toward the improvement of the thermal performance of the building envelope, thereby contributing to increase the energy efficiency of the built environment. In this context, an increasing number of studies are focusing on the development of mortars with enhanced thermal performance, i.e., thermal insulating mortars. However, considering the innovative character of these materials, reliable data on their long-term performance is still lacking, particularly concerning the thermal performance and suitability to refurbishment works. The aim of this paper is to evaluate the long-term thermal conductivity and biological colonisation of industrially produced and experimentally designed thermal mortars with EPS, cork and silica aerogel aggregates. The long-term performance of the mortars was assessed prior, during and after exposure to three accelerated ageing tests including elevated temperature, freeze–thaw cycles and high humidity levels. For each test, an empirical model (i.e., Arrhenius law, Peck model, and Coffin-Manson equation) was used to compute the acceleration factor, thus allowing to correlate the accelerated and natural ageing results and to estimate the degradation levels that would be obtained after 10 years of exposure to natural weather conditions. The results of the thermal conductivity show that a maximum increase of 10 % and 30 % can be obtained after ageing for the industrially produced and experimentally designed mortars, respectively. Moreover, all mortars were susceptible to mould growth, with the greatest biological colonisation levels obtained after the high moisture content ageing for the experimentally designed mortars.

1. Introduction

The existence of a major climate and energy crisis of anthropogenic origin is now undoubtedly agreed upon by the scientific community. To address this issue, described by the United Nations as a "direct existential threat to humanity" [1], the European Commission has set an ambitious goal of net zero emission by 2050 [2]. The construction industry is particularly targeted since it accounts for 40 % of European energy consumption and 36 % of the energy related to greenhouse gas emissions [3]. It is therefore of upmost importance to implement innovative eco-efficient solutions to mitigate this impact, in particular by improving the thermal performance of the building envelope. In this context, an increasing number of studies are focusing on the development of mortars with enhanced thermal performance, i.e., thermal insulating mortars, or, in a simplified way, thermal mortars. Nevertheless, there is still a lack of data related to the performance and long-term durability of these innovative construction and building materials.

The general principle of a thermal mortar formulation is to replace a volume of conventional aggregates (e.g., sand) with lightweight aggregates presenting lower thermal conductivity. Among the most commonly used materials are expanded polystyrene (EPS) [4–9], expanded clay [8], expanded cork [6–10], silica aerogel [4,5,8,10,11],

* Corresponding author at: LNEC, National Laboratory for Civil Engineering, Av. do Brasil, 101, 1700-066 Lisbon, Portugal.
E-mail address: jparracha@lnec.pt (J.L. Parracha).

https://doi.org/10.1016/j.enbuild.2024.114403
Received 19 December 2023; Received in revised form 29 May 2024; Accepted 6 June 2024
Available online 11 June 2024

perlite [12] or expanded glass [13]. The incorporation of these lightweight aggregates in sufficient quantities allows to obtain a mortar with an enhanced thermal performance compared to a conventional mortar. Some admixtures, such as air entraining agents, are commonly added in industrial thermal mortars, to contribute for the reduction of their thermal conductivity. According to the European standard EN 998-1:2017 [14] a thermal mortar should have the following characteristics: (i) a thermal conductivity lower than 0.2 W/(m.K) at 10 °C; (ii) a capillary water absorption coefficient lower than 0.40 kg/(m^2.$min^{0.5}$); (iii) a water vapour diffusion resistance coefficient lower than 15; and (iv) a compressive strength between 0.4 and 5 N/mm^2.

Thermal mortars are currently being used for enhancing the thermal performance of the building envelope in both new construction and retrofitting of façades. As a result, previous studies have focused on the optimisation of the thermal behaviour of these mortars. By increasing the volume proportion of EPS or cork aggregates (up to 85 % and 80 %, respectively), Gomes et al. [6] achieved a reduction of thermal conductivity up to 80 % when compared to the reference mortar, with the thermal mortars presenting thermal conductivity values of approximately 0.2 W/(m.K). Moreover, Pedroso et al. [11] obtained a mortar with a thermal conductivity lower than 0.03 W/(m.K) using silica aerogel replacing sand, whereas Parracha et al. [8] evaluated the thermophysical performance of three commercially available and five experimentally designed lightweight thermal mortars with different percentages of aggregates (i.e., expanded cork, EPS, expanded clay, and silica aerogel) and obtained thermal conductivity values ranging between 0.08 W/(m.K) and 0.15 W/(m.K).

According to the studies mentioned above, thermal insulating mortars exhibit promising physical properties, such as low thermal conductivity and high-water vapour permeability. Additionally, they possess unique characteristics that distinguish them from other commonly used thermal insulation products, like thermal insulation boards. For example, Posani et al. [15] highlighted that thermal mortars are particularly suitable for retrofitting old walls in historic buildings. Their pasty state when freshly mixed allows for easier application on irregular or uneven surfaces [15–18]. Moreover, research by Vyšvařil et al. [12] and Pavlík et al. [13] on lime-based thermal mortars with perlite or expanded glass aggregates demonstrated that these materials yield high-thermal-performance renders that are physically and chemically compatible for refurbishing heritage buildings.

However, all of the previously mentioned studies used mortars in unaged conditions to determine their properties. In fact, mortars' long-term performance can be affected due to the ageing of the material, caused by the possible synergistic effect of several degradation agents over time (e.g., moisture [5,6,19,20], extreme temperatures [21,22], wind, solar radiation [10], pollution or biological colonisation [23]).

Gomes et al. [5] showed that the thermal conductivity of mortars experimentally produced with EPS aggregates and silica aerogel significantly increased with moisture content, following an exponential law. In parallel, the authors [6] identified a similar trend considering thermal mortars with cork aggregates, reporting a 3-fold increase of thermal conductivity between the dry state and the saturated state (from 0.23 W/(m.K) to 0.69 W/(m.K)). Additionally, by investigating the thermal performance of fibrous aerogel samples under different hygrothermal environments, Lakatos et al. [19] found that high levels of water vapour led to a significant decrease in the thermal conductivity of the materials tested. In fact, water is frequently identified as the main degradation agent of mortars [24], as with most of construction materials, influencing several degradation mechanisms, such as the freeze–thaw behaviour [7] or biological colonisation [25]. When freezing, the water contained in the inner pores of the mortar causes significant internal pressure by expanding, leading to the formation of cracks and therefore decreasing mechanical resistance and increasing water absorption. Being a powerful solvent [26], it can also cause the leaching of the material or conversely facilitate the penetration of aggressive chemical agents (e.g., chlorides, sulphates) through capillary networks and cracks. Furthermore, Parracha et al. [23] have pointed out that moisture significantly increases the risk of biological growth, possibly resulting in aesthetic alteration of the façades when the mortar is used as thermal insulation layer in External Thermal Insulation Composite Systems (ETICS) and increasing water retention, thus causing further deterioration.

Some degradation mechanisms have slow kinetics and have thus significant effects only after a long period of time [10]. It is therefore necessary to examine the long-term behaviour of the materials in order to accurately assess their performance and durability. Yet, monitoring the properties of a naturally aged material over several decades is often impossible due to the long-time span involved. To overcome this issue, accelerated ageing methods [28] using empirical laws can be used in laboratory. These methods consist of exposing the material to extreme environmental conditions in comparison to those that occur naturally, which makes it possible to obtain levels of degradation potentially equivalent to several decades of ageing in a matter of weeks or months. It is worth mentioning that these methods do not provide universal results, but rather an indication of the behaviour of the material in climatic conditions corresponding to a specific geographical area. Furthermore, many ageing phenomena exist in real-life conditions, and it is impossible to make an exhaustive study of all of them simultaneously.

Using these methods, Berardi et al. [10] evaluated the performance of mortars with varying amounts of silica aerogel before and after being subjected to freeze–thaw cycles, high temperatures and high relative humidity levels equivalent to 20 years of natural ageing in Canada. Despite the increase in the thermal conductivity of each material tested, the authors concluded that specimens with large amounts of aerogel preserved their properties after ageing. Similarly, Lakatos et al. [22] used elevated temperature accelerated ageing and empirical models to investigate the stability of the thermal performance of aerogel blankets over 10 years of service time and noted excellent conservation of their thermal properties. Parracha et al. [23] studied the influence of UV exposure, air pollutants (SO_2) and hygrothermal cycles on the long-term durability of ETICS with thermal insulation boards and observed physical and aesthetic degradation after ageing. In particular, the authors observed that hygrothermal cycles significantly affected the surface properties of ETICS, thus favouring biological colonisation. In order to investigate the influence of freezing mechanisms on the durability of thermal mortars, Maia et al. [7] exposed samples containing EPS and cork to heating-freezing, humidification-freezing and freeze-thawing cycles, and observed a noticeable alteration of the mortar matrix and an increase of water vapour permeability.

Only a few thermal insulation materials have yet been studied using accelerated ageing methods, and data on the durability of thermal mortars is therefore lacking so far. This paper aims to evaluate the long-term thermal conductivity and susceptibility to biological colonisation of thermal insulating mortars incorporating EPS, cork and silica aerogel aggregates. Three accelerated ageing factors were calculated to correlate accelerated ageing results with real life exposure in Lisbon, Portugal. Accelerated ageing tests include exposure to high temperature, freeze–thaw cycles and high relative humidity levels. The results herein obtained intend to contribute to further understand the influence of different degradation agents and mechanisms on the durability of innovative thermal insulating mortars. As such, they provide additional insight for the evaluation of their efficiency as a sustainable thermal insulation material.

2. Materials

Four thermal mortars were tested: (i) an industrially produced mortar with silica aerogel aggregates (A^{AER}); (ii) a commercially available mortar with EPS aggregates (B^{EPS}); (iii) an experimentally designed mortar with natural hydraulic lime 3.5 (NHL 3.5) as binder and sand and cork as aggregates (C^{CORK}); and (iv) a reference NHL 3.5 and sand mortar without lightweight aggregates (D^{REF}). The lightweight

aggregates and the matrix of the four mortars can be observed in the surface photographs of the samples shown in Fig. 1, which were obtained using an Olympus SZH10 stereomicroscope at ×7 magnification.

For the industrially produced A^{AER} mortar, the exact composition is unknown due to industrial confidentiality. However, it is known to be a cement-based mortar composed of a blend of mineral binders, rheological agents, resin, hydrophobic agents, and a commercially available supercritical hybrid silica aerogel. According to the technical datasheet of the silica aerogel [29], this product has a particle size of ≤3500 μm, an apparent density of ≤90 kg/m^3, a particle compressive strength of ≤0.80 MPa, and a thermal conductivity of ≤0.020 W/(m.K). Additionally, a previous study using a similar aerogel mortar [11], reported that the mineral binders represent approximately 20 % by weight of the mixture, silica aerogels about 37 %, with the remaining percentage allocated to other components. A water/powder ratio of 1.33 in mass was used for the mortar preparation to obtain a good workability.

According to the technical datasheet, mortar B^{EPS} was formulated with lime, EPS aggregates, mineral aggregates and special additives. This mortar was produced by the same manufacturer as A^{AER}, and its exact formulation is also unavailable due to industrial confidentiality. According to the technical datasheet, this mortar should be mixed using 5.5 to 6 L of kneading water per 4.6 kg bag of powder, resulting in a water-to-powder mass ration of 1.2 to 1.3. Although the volume proportion and the diameter of the lightweight aggregates are not specified in the technical datasheet, stereomicroscope observations (Fig. 1) of the samples estimate the diameter of the EPS beads to range between 1 mm and 2 mm.

Table 1 presents the values of some mechanical and hygrothermal properties either declared by the manufacturers in technical data sheets (i.e., for B^{EPS}) or collected from previous studies [5] characterising similar (i.e., for A^{AER}) [11] or the same mortars (i.e., for C^{CORK} and D^{REF}) [30].

Table 1
Mechanical and hygrothermal properties of the mortars according to technical data sheets and previous studies.

	A^{AER}	B^{EPS}	C^{CORK}	D^{REF}
Dry bulk density (kg/m^3)	165 ± 11	150 ± 5	1175 ± 38	1748 ± 28
Water vapour permeability μ (–)	7.8 ± 0.1	≤5.0	7.0 ± 0.1	8.8 ± 0.1
Capillary water absorption A_w (kg/(m^2.min$^{0.5}$))	1.00 ± 0.04	<0.400	1.30 ± 0.20	2.78 ± 0.05
Compressive strength (MPa)	0.227 ± 0.002	≥0.400	0.300 ± 0.080	0.500 ± 0.100
Flexural strength (MPa)	0.099 ± 0.004	≥0.250	0.110 ± 0.060	0.260 ± 0.020

The experimentally designed mortars were prepared with a binder (NHL 3.5)/aggregate volumetric ratio of 1:3 using a 50 % replacement of sand by cork aggregates in the case of mortar C^{CORK} and 100 % sand for the reference mortar (D^{REF}). The water / binder ratio (1.7) was optimised by experimental applications to obtain a good workability. The bulk density values of the mortar components were determined in accordance with EN 1097-3:1999 [31] and are the following: natural hydraulic lime (NHL 3.5) – 687 kg/m^3; sand – 1452 kg/m^3; and expanded cork – 225 kg/m^3. Moreover, the particle size of the cork aggregates ranged between 1 mm and 2 mm. The grain size of the sand was between 0 and 4 mm, according to the technical data sheet.

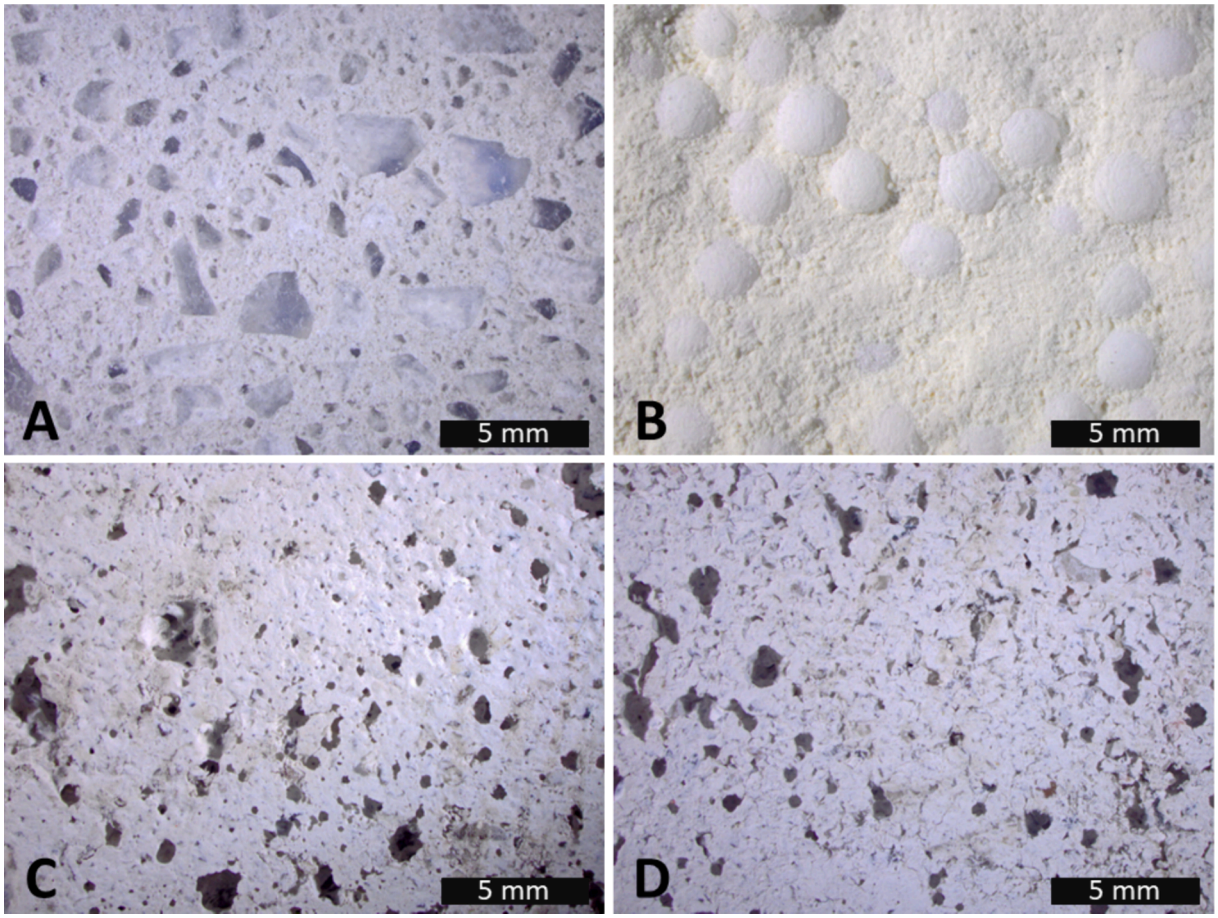

Fig. 1. Optical microscope images of the mortars A^{AER} (A), B^{EPS} (B), C^{CORK} (C) and D^{REF} (D).

3. Methods

3.1. Accelerated ageing procedures

Accelerated ageing methods were used to allow for the assessment of the long-term properties of the thermal mortars while conducting this study on a reasonable time scale. Among the multiple degradation mechanisms that occur in natural outdoor conditions, the effects of elevated temperature, freeze–thaw and elevated relative humidity levels were evaluated. In order to measure their specific influence, the three accelerated ageing procedures were conducted separately on different specimens. The acceleration of the degradation is obtained by exposing the specimens to intense climatic conditions (i.e., temperature, humidity) with respect to those that naturally occur in the geographical area of reference, namely Lisbon, Portugal. For each mechanism, an empirical law (e.g., Arrhenius law [28], the Peck model [32] or the Coffin-Manson equation [33]) was used to calculate the acceleration factor, which is defined as the ratio between the reaction rates under accelerated ageing and natural ageing conditions. These factors allowed to estimate the required duration of the ageing procedures to induce degradation equivalent to a reference number of years in natural weathering conditions. Considering the lack of studies on the assessment of the long-term performance of innovative thermal mortars, the ageing procedures were designed to be equivalent to 10 years of ageing in outdoor natural conditions. The following sections detail the specific methods used for each accelerated ageing test.

3.1.1. Elevated temperature ageing

Considering a microscopic scale, the rise in temperature of a material results in an increase in the energy of the molecular motion. Collisions between molecules are thus favoured, which accelerates degradation reactions [34]. The relationship between the reaction rate k and temperature T can be expressed using the Arrhenius' empirical law [28] (Eq. (1)).

$$k(T) = A \bullet \exp\left(-\frac{E_a}{RT}\right) \quad (1)$$

In the equation above, E_a is the activation energy of the reaction in J/mol, R is the perfect gas constant (R = 8.314 J/(mol.K)), T is the material's temperature in Kelvin and A is a constant of proportionality.

The specimens were vertically placed in a mechanical convection oven from Cassel (Fig. 2.A) set at a constant temperature of $T_{ag} = 70^{\circ}C$. According to previous studies for different insulation materials (e.g., [10,28]) the temperature value adopted herein is sufficient to cause substantial ageing without triggering unrealistic degradation mechanisms.

The acceleration factor f_T can therefore be expressed as a function of T_{ag} (accelerated ageing temperature) and T_{nat} (use condition temperature) in accordance with Eq. (2):

$$f_T = \frac{k(T_{ag})}{k(T_{nat})} = \exp\left(-\frac{E_a}{R}\left(\frac{1}{T_{ag}} - \frac{1}{T_{nat}}\right)\right) \quad (2)$$

Considering that thermal mortars are usually applied as thermal insulation layer in a defined type of External Thermal Insulation Composite System (ETICS) [35], it was assumed that in use conditions the temperature of the mortars is close to the outdoor temperature. In fact, thermal mortars are not applied as the finishing layer in direct contact with the outside environment. Instead, this function is performed by a rendering system consisting of a reinforced base coat and a finishing coat. This outer layer is exposed to the outside environment, achieving higher surface temperatures and thereby protecting and reducing the average temperature of the underlying thermal mortar. Therefore, T_{nat} was calculated to be 17.2 °C by averaging the daily temperatures registered in Lisbon, Portugal in the year of 2020, according to the data provided by the Portuguese Institute for Sea and Atmosphere (IPMA). According to Jelle et al. [28] the value of the activation energy E_a was taken equal to 70 kJ/mol and was considered temperature independent.

An acceleration factor of 84 was calculated (Table 2), thus indicating a required exposure time of 43 days in elevated temperature ageing to be equivalent to 10 years of outdoor natural ageing.

3.1.2. High moisture content ageing

As previously mentioned, water plays a major role in several degradation mechanisms, such as leaching, freeze–thaw cycles, or penetration of aggressive agents [24].

In order to measure the influence of high humidity levels on the long-term performance of thermal mortars, the specimens were placed in an ARALAB FC700EDTU climatic chamber, in which the humidity and temperature were kept constant. To obtain a sufficiently high acceleration factor, the relative humidity value was set at the highest value (80 % RH) allowing proper continuous operation of the climatic chamber (i.

Table 2
Acceleration factors and accelerated ageing time equivalent to 10 years of outdoor natural conditions.

Ageing procedure	Acceleration factor	Number of days in accelerated ageing equivalent to 10 years of outdoor natural ageing
Elevated temperature	84	43
High moisture exposure	56	65
Freeze-thaw behaviour	270	14

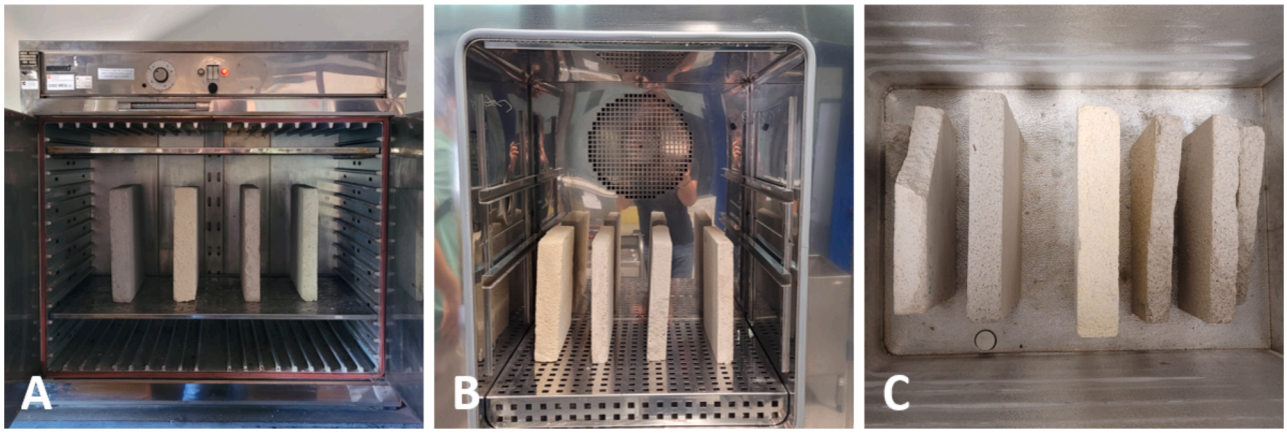

Fig. 2. Sample disposition in the accelerated ageing tests: elevated temperature ageing (A), high humidity ageing (B), and freeze–thaw ageing (C).

e., constant and homogeneous relative humidity level and absence of liquid water accumulation) throughout an extended experimental period. Additionally, the temperature was set at 60 °C to raise the partial water vapour pressure and promote sample degradation. The specimens were vertically placed on a metal grid (Fig. 2B) to ensure that all their faces are in direct contact with the climatic chamber environment air and to allow homogeneous humidification.

The Peck model [10,32] evaluates the correlation between the moisture content and the degradation rate and was used to calculate the acceleration factor f_{RH} considering the high humidity levels (Eq. (3)):

$$f_{RH} = \left(\frac{RH_{ag}}{RH_{nat}}\right)^{m} \tag{3}$$

In the above equation, RH_{ag} is the humidity level inside the climatic chamber (80 %), RH_{nat} is the average humidity considering outdoor natural conditions, and m is the Peck coefficient, which depends on the activation energy. Extrapolating Peck's results by linear regression ($R^2 = 0.96$), m was taken equal to 3.53 for an activation energy $E_a = 70\text{kJ/mol}$. The average relative humidity in Lisbon, Portugal in the year of 2020 RH_{nat} was calculated to be 72 %, according to the data provided by IPMA. Since the climatic chamber is set at a temperature of 60 °C, the acceleration of degradation caused by temperature should also be taken into account (Eq. (4), assuming $T_{ag} = 60^{\circ}\text{C}$, and $T_{nat} = 17.2^{\circ}\text{C}$ (see Section 3.1.1)). The overall acceleration factor is therefore calculated according to Eq. (4):

$$f_{RH,T} = f_{RH} f_T = \left(\frac{RH_{ag}}{RH_{nat}}\right)^{m} \exp\left(-\frac{E_a}{R}\left(\frac{1}{T_{ag}} - \frac{1}{T_{nat}}\right)\right) \tag{4}$$

This value was equal to 56 (Table 2), thus indicating a required exposure time of 65 days in high moisture content ageing to be equivalent to 10 years of outdoor natural ageing.

3.1.3. Freeze-thaw ageing

Temperature fluctuations are also a significant factor of degradation. Indeed, most materials dilate when their temperature increases, which can induce significant internal stresses. In the case of mortars, this phenomenon becomes more severe when temperatures are fluctuating from below to above 0 °C, causing the water contained in the inner pores of the material to successively freeze and thaw [7]. It is possible to accelerate the degradation caused by this phenomenon by artificially enlarging the temperature range to which the mortars are exposed compared to what would naturally occur. The specimens were therefore alternatively placed in an oven from Micrometrics set at 60 °C and in a freezer from Bauknecht set at −15 °C (Fig. 2C). In order to expose the samples to 48 h-cycles of freeze–thaw, they were displaced manually from the oven to the freezer and conversely every 24 h.

The acceleration factor resulting from this type of degradation mechanism is calculated using the Coffin-Manson equation [33] (Eq. (5)).

$$f_{FT} = \left(\frac{\Delta T_{ag}}{\Delta T_{nat}}\right)^{n} \tag{5}$$

Where ΔT_{ag} is the temperature difference set in the freeze–thaw climatic chamber ($\Delta T_{ag} = 75^{\circ}C$), ΔT_{nat} is the average daily temperature difference experienced in outdoor conditions, and n is the Coffin-Manson parameter. Using data provided by IPMA for the year 2020 in Lisbon, Portugal, ΔT_{nat} was calculated to be 11.6 °C. The Coffin-Manson parameter (n) was taken to be 3 [10].

An acceleration factor of 270 (Table 2) was obtained for the freeze–thaw ageing, representing a required exposure time of 14 days to be equivalent to 10 years of use. In fact, this particularly high value of the acceleration factor could be expected due to Lisbon's climate, which is less severe when compared to other European countries.

3.2. Durability assessment

To evaluate the durability of the thermal mortars, the present study focused on three characteristics: overall appearance of the mortars, thermal conductivity and susceptibility to biological colonisation.

3.2.1. Visual observation

In order to identify any visible degradation marks on the surface of the samples, visual observations were performed by optical microscopy before and after the accelerated ageing tests. These observations were carried out using an Olympus SZH10 microscope, with adjustable magnification between x7 and x90, thus allowing the observation of potential surface alterations caused by ageing (e.g. discolouration, defacement or surface cracks) at different scales.

3.2.2. Thermal conductivity

Thermal conductivity measurements were carried out using the heat flow meter steady-state method, according to EN 12667:2001 [36]. The method consists of placing test samples between a cold plate and a hot plate to establish a temperature gradient in the mortar, thus creating a heat flux through the test sample. Once steady state is reached, the heat flux is measured, which allows the thermal conductivity to be calculated using the Fourier's law (Eq. (6)).

$$q = \frac{\lambda}{e}(T_h - T_c) \tag{6}$$

In the Eq. (6), q is the heat flux in W/m^2, λ is the thermal conductivity in W/(m.K), T_h and T_c are the respective temperatures of the hot and cold plates in Kelvin and e is the thickness of the sample. The heat flux measurements were carried out using a Heat Flow Meter Instrument Holometrix rapid-K, whereas the thickness of the samples was determined by manual measurement in accordance with the standard EN 823:2013 [37].

Thermal conductivity measurements were performed on squared samples with area of 300 mm x 300 mm to comply with the requirements of the heat flow meter equipment. The thickness of the samples was controlled to be approximatively 50 mm, which corresponds to a typical application thickness for thermal mortars and other thermal insulation materials in southern European countries like Portugal. To monitor the long-term behaviour of the mortars, the measurements were performed prior, during and after the ageing procedures. Therefore, two intermediate measurements were carried out for each test, at approximately one third and two thirds of their duration, i.e., after 14 days and 28 days for elevated temperature, after 23 days and 48 days for elevated humidity, and after 5 days and 9 days for the freeze–thaw.

The thermal conductivity of the unaged samples was determined after stabilisation in a climatic chamber at 23 °C and 50 % RH. As the temperature and moisture conditions were quite different between ageing procedures, the samples were placed for two days in a chamber conditioned at 23 °C and 50 % RH prior to each intermediate measurement to uniformize initial thermal conductivity test conditions. Moreover, in order to consider the effect of humidity and temperature variations on the measured values of thermal conductivity, the equation defined in ISO 10456:2007 [38] was used (Eq. (7)):

$$\lambda_c = \lambda_m F_T F_u F_a \tag{7}$$

Where λ_c is the value of thermal conductivity corrected according to the reference conditions (23 °C, 50 % RH), λ_m is the measured value of thermal conductivity, and F_T, F_u, and F_a are the correction factors for temperature, moisture, and ageing variations between the test conditions and the reference conditions, respectively. Since the measurements were taken only a few weeks apart and the mortars were kept in laboratorial conditions, the effect of natural ageing was disregarded [5,38] and F_a was therefore taken to be equal to 1. The factors F_T and F_u were

estimated in accordance with Eq. (8) and Eq. (9) respectively:

$$F_T = \exp[f_T(T_{23,50} - T_m)] \quad (8)$$

$$F_u = \exp[f_u(U_{23,50} - U_m)] \quad (9)$$

In the above equations, $T_{23,50}$ and $U_{23,50}$ are the temperature (in Kelvin) and the volume moisture content (in m^3/m^3) of the sample during the measurement of reference (unaged state), T_m and U_m are the temperature and volume moisture content of the sample during the measurement, f_T and f_U are conversion factors for temperature and moisture, respectively. The temperature values (i.e., T_m and $T_{23,50}$) were measured automatically by the Holometrix equipment during the thermal conductivity measurements, whereas the values of volume moisture content (U_m and $U_{23,50}$) were calculated from the volume (V, in m^3) and mass of the samples weighted before the measurement (m_i, in kg) and in the dry state (m_{dry}), according to Eq. (10):

$$U_i = \frac{(m_i - m_{dry})}{\rho_{water} V} \quad (10)$$

Where i indicates the set of conditions considered (e.g., $i =$ 23 °C, 50% RH) and ρ_{water} is the density of the water (1000 kg/m^3). The values of the correction factors were taken equal to 0.003 for f_T and 4 for f_U, according to ISO 10456 [38] and using the standard values for lightweight concrete [5].

3.2.3. Biological colonisation

The susceptibility to biological colonisation in the mortars was assessed following a method previously adapted and validated for ETICS by Parracha et al. [27]. Before conducting the test, three 40 mm side cubic samples of each mortar were cut from the specimens previously used for thermal conductivity measurements. These samples were steam sterilised and placed in culture flasks containing culture media prepared with 4 % malt and 2 % agar. Then, 2 mL of a mixed spore suspension of two fungal species: *Aspergillus niger* Tiegh. and *Penicillium funiculosum* (De Bary) G. Arnaud, was uniformly applied on the samples and culture media. The test flasks were placed for four weeks in a culturing chamber at a temperature (T) between 28 °C and 30 °C and a relative humidity (RH) higher than 90 % [39]. The biological colonisation rate was visually assessed weekly using the guidelines provided in the standard ASTM D5590-17 [39]: 0 – no visible growth (0 % of contaminated surface); 1 – traces of growth (less than 10 % of contaminated surface); 2 – light growth (between 10 % and 30 % of contaminated surface); 3 – moderate growth (between 30 % and 60 % of contaminated surface) and 4 – heavy growth (more than 60 % of contaminated surface). After four weeks of testing, all the samples were carefully removed from the culture flasks to perform the final assessment of the biological colonisation rate. This assessment was carried out using an Olympus SZH10 optical microscope to ensure precision and validate the results obtained during the weekly intermediate assessments. Three replicates of Whatman n°1 filter paper were used as control to validate the test results.

4. Results

4.1. Unaged mortars

4.1.1. Thermal conductivity

Considering that variations in thermal performance induced by ageing could be relatively low [10], thermal conductivity measurements were carried out on each specimen in the unaged state after mass stabilisation at 23 °C and 50 % RH, to consider the possible slight variations obtained between samples from the same mortar type. Therefore, these values (Table 3) were subsequently used as reference for the initial state for each ageing test, thus allowing to pinpoint variations in thermal conductivity solely attributable to the accelerated ageing cycles. The following average results were obtained: A^{AER} – 0.0324 ± 0.00120 W/(m.K); B^{EPS} – 0.0544 ± 0.00200 W/(m.K); C^{CORK} – 0.210 ± 0.0142 W/(m.K) and D^{REF} – 0.426 ± 0.0182 W/(m.K). The manufactured mortars have shown better thermal performance if compared to the experimentally designed mortars, presenting values of thermal conductivity lower than 0.1 W/(m.K) (class T1 according to standard EN 988-1 [14]). Nevertheless, C^{CORK} and D^{REF} cannot be classified as thermal mortars in accordance with EN 998-1 [14] requirements, due to their greater thermal conductivity ($\lambda > 0.2$ W/(m.K), which is the threshold adopted for class T2).

Table 3
Thermal conductivity (W/(m.K)) results of the unaged mortars used for the elevated temperature, high moisture and freeze–thaw ageing tests.

Ageing procedure*	Thermal conductivity (unaged state) [W/(m.K)]			
	A^{AER}	B^{EPS}	C^{CORK}	D^{REF}
Elevated temperature	0.0320	0.0563	0.219	0.447
High moisture	0.0338	0.0546	0.218	0.419
Freeze-Thaw	0.0314	0.0523	0.194	0.412
Average results of thermal conductivity	0.0324 ± 0.00120	0.0544 ± 0.00200	0.210 ± 0.0142	0.426 ± 0.0182

*The measurements were performed after mass stabilization of the samples in a conditioned room at 23 °C and 50 % RH.

4.1.2. Biological colonisation

The biological colonisation tests carried out on the unaged samples showed that all mortars were susceptible to mould growth. Fig. 3 shows the average results of the mould growth assessment carried out each week on the unaged tested samples.

Biological colonisation assessment showed light traces of mould growth from the first week onwards on all tested mortars (Fig. 4 **and Supplementary Material**). During the first two weeks, the predominant colonising microorganism was identified as being *A. niger* for A^{AER}, C^{CORK} and D^{REF} mortars and *P. funiculosum* for B^{EPS}. The rate of mould growth was slower after the second week in the case of mortars A^{AER} and B^{EPS}, whose final average biological colonisation rate did not reach 2 out of 4 (i.e., light mould growth) at the end of the test.

4.2. Elevated temperature ageing

4.2.1. Visual assessment

As previously stated, all samples were visually inspected before the thermal conductivity measurements to identify any possible degradation marks. Mortar C^{CORK} showed a brittle behaviour, breaking into four pieces after the first thermal conductivity measurement (i.e., after 14 days of elevated temperature ageing, corresponding to 3 years of natural ageing), making it impossible to continue with the long-term thermal conductivity assessment (Fig. 5A). The remains of the mortar continued to undergo the accelerated ageing procedure in order to carry out the biological colonisation assessment at the end of the elevated temperature ageing. After 30 days in elevated temperature (i.e., corresponding to ~7 years of natural ageing), the formation of some plaques consisting of agglomerates of deformed EPS beads was observed on the surface of B^{EPS} (Fig. 5B), probably due to the pressure of the plates in the thermal conductivity tests. Additionally, it was possible to observe slight surface defacements on mortar D^{REF} during the elevated temperature ageing (Fig. 5C). On the other hand, mortar A^{AER} have not shown any visible signs of degradation.

4.2.2. Long-term thermal conductivity

Fig. 6 shows the trend of the thermal conductivity of the mortars during the elevated temperature ageing. The thermal conductivity of all the samples increased between the initial and the final states of the procedure but followed different trends. A non-linear trend was observed for A^{AER}, whose loss of thermal performance occurred mainly

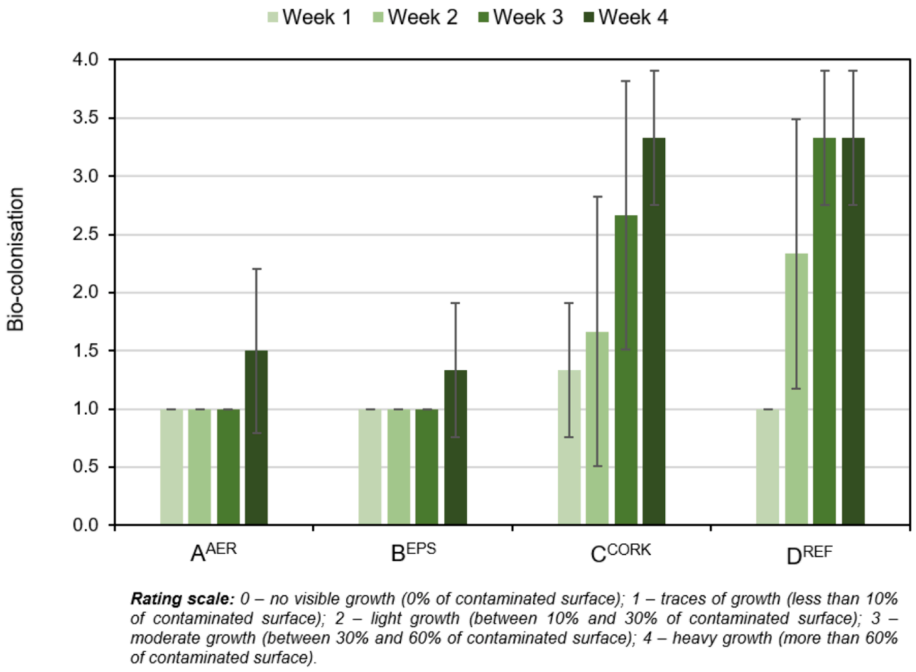

Fig. 3. Average rate of mould growth on A^{AER}, B^{EPS}, C^{CORK} and D^{REF} samples in the unaged state.

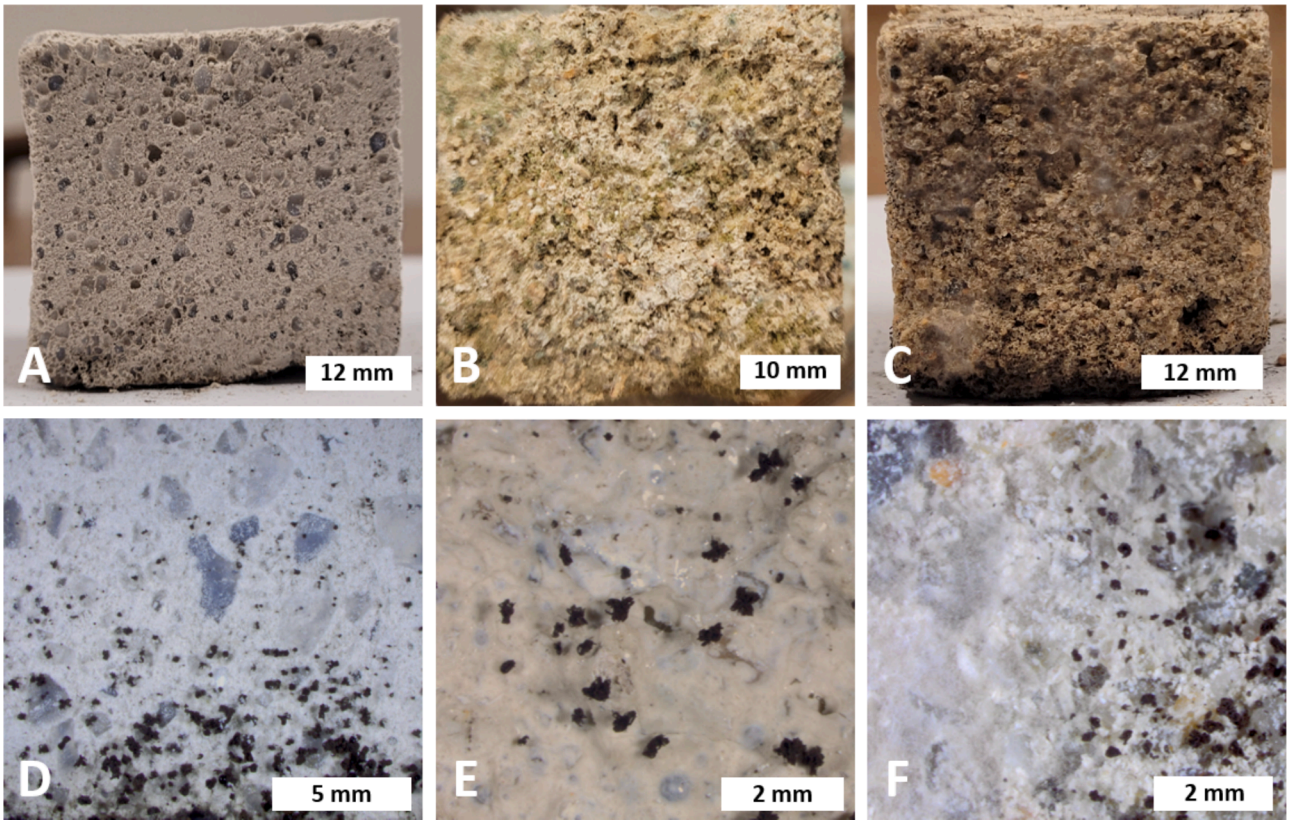

Fig. 4. Visual observations of the unaged mortars after the biological colonisation tests: A^{AER} (A); C^{CORK} (B); D^{REF} (C) and stereomicroscope images: A^{AER} (D); C^{CORK} (E); D^{REF} (F).

during the first few years of ageing: its thermal conductivity increased from 0.0320 W/(m.K) to 0.0341 W/(m.K) in 3 years (+6.6 %), then reached only 0.0346 W/(m.K) after 10 years (8.1 % increase if compared to the initial unaged state). A more complex behaviour was observed for B^{EPS}, whose thermal conductivity went through a maximum of 0.0621 W/(m.K) after 3 years of ageing (10.3 % increase) and then stabilised at a slightly lower value of 0.0607 W/(m.K), i.e. 8 % higher compared to the unaged state. C^{CORK} also underwent a significant increase in thermal conductivity after 3 years of natural ageing (from 0.219 W/(m.K) to 0.262 W/(m.K)), but it was not possible to depict a trend due to the

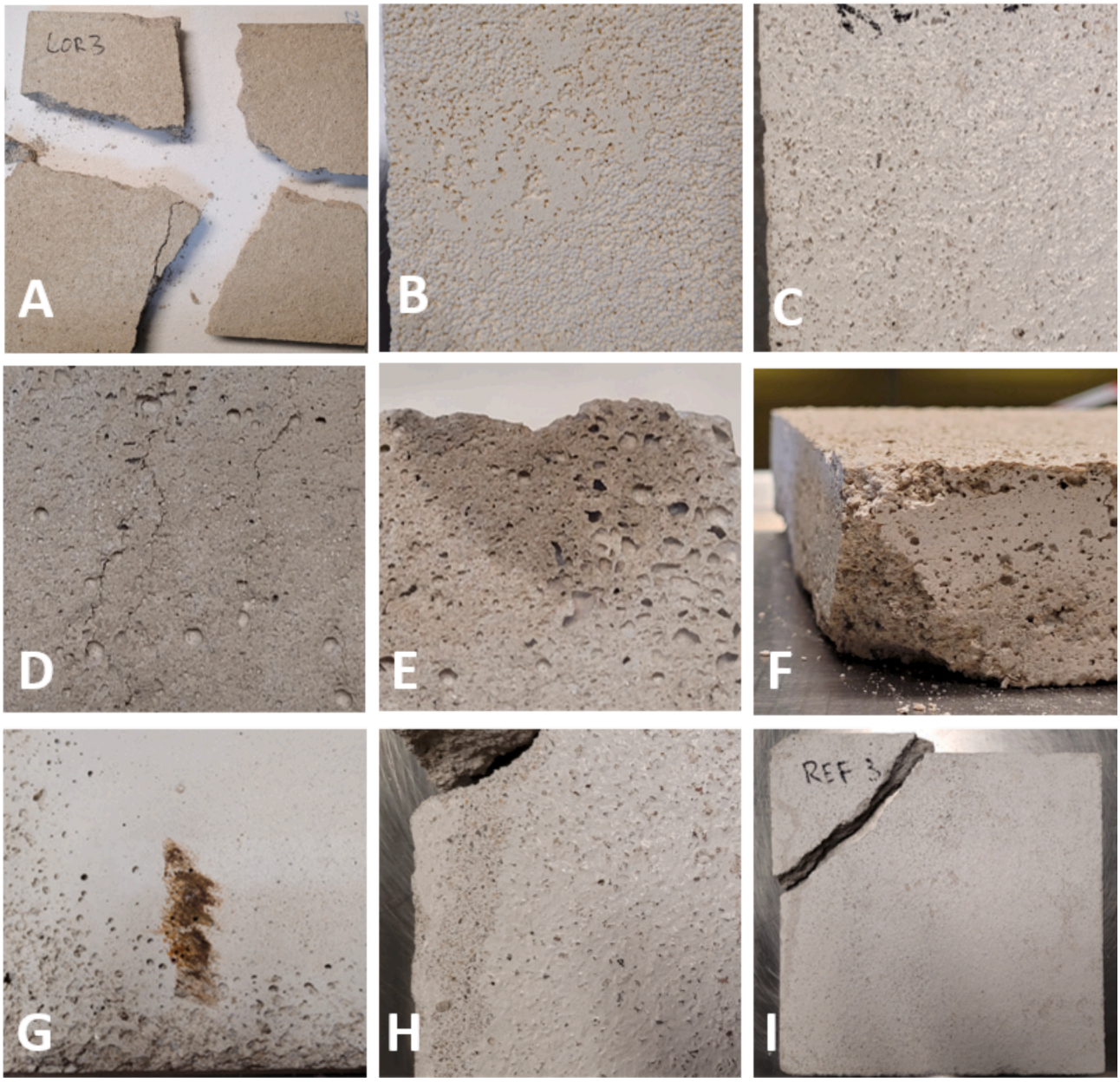

Fig. 5. Visual observations of the mortars during the ageing tests: elevated temperature (C^{CORK}, after 3 years of ageing (A); B^{EPS}, after 7 years of ageing (B); D^{REF}, after 10 years of ageing (C)), high moisture (A^{AER}, after 3 years of ageing (D) and (E); D^{REF}, after 10 years of ageing (F)) and freeze–thaw (C^{CORK}, after 4 years of ageing (G); D^{REF}, after 10 years of ageing (H) and (I)).

reduced number of measurements (Section 4.2.1). Moreover, the thermal conductivity of D^{REF} increased from 0.447 W/(m.K) to 0.577 W/(m.K) (+29 %) in 7 years of ageing, following a similar trend as that of A^{AER} (Fig. 6), with a higher rate of increase during the first years of ageing.

Table 4 shows the mathematical models selected to describe the evolution of the thermal conductivity (λ) as a function of the equivalent number of years in natural ageing (y). Given the restricted number of experimental values measured for each mortar, it is important to emphasise that these equations are intended to facilitate the interpretation of results rather than to establish a physical law enabling precise prediction of the observed ageing phenomena. In elevated temperature ageing, results show an exponential increase of thermal conductivity with ageing for mortars A^{AER} ($R^2 = 0.998$) and D^{REF} ($R^2 = 0.999$) (Fig. 6; Table 4), thus indicating a significant loss of thermal performance in the first few years of ageing, followed by a gradual stabilisation. Considering the exponential model (Table 4), it is possible to observe that the limit value (i.e., maximum thermal conductivity) of mortar A^{AER} is 8.1 % higher than that obtained in unaged conditions, with a characteristic degradation time (i.e., the duration after which 63 % of the total variation of thermal conductivity is reached, noted τ) of only 2 years. Moreover, the model shows that 63 % and 95 % of the increase in thermal conductivity is likely to occur in the first 2 and 6 years after application, respectively [30]. Regarding mortar D^{REF}, the thermal conductivity undergoes a significantly greater variation (i.e., the limit value is 31 % higher if compared to unaged conditions), showing a characteristic time of 2.7 years. In this case, 95 % of the thermal conductivity increase is observed in the first 8 years of natural ageing.

However, identifying behaviour trends from the data obtained for B^{EPS} and C^{CORK} mortars proved more challenging. The peak in thermal conductivity reached by B^{EPS} after 3 years of natural ageing prevented the development of a meaningful model with a good determination coefficient. By considering the possibility that this value could be an

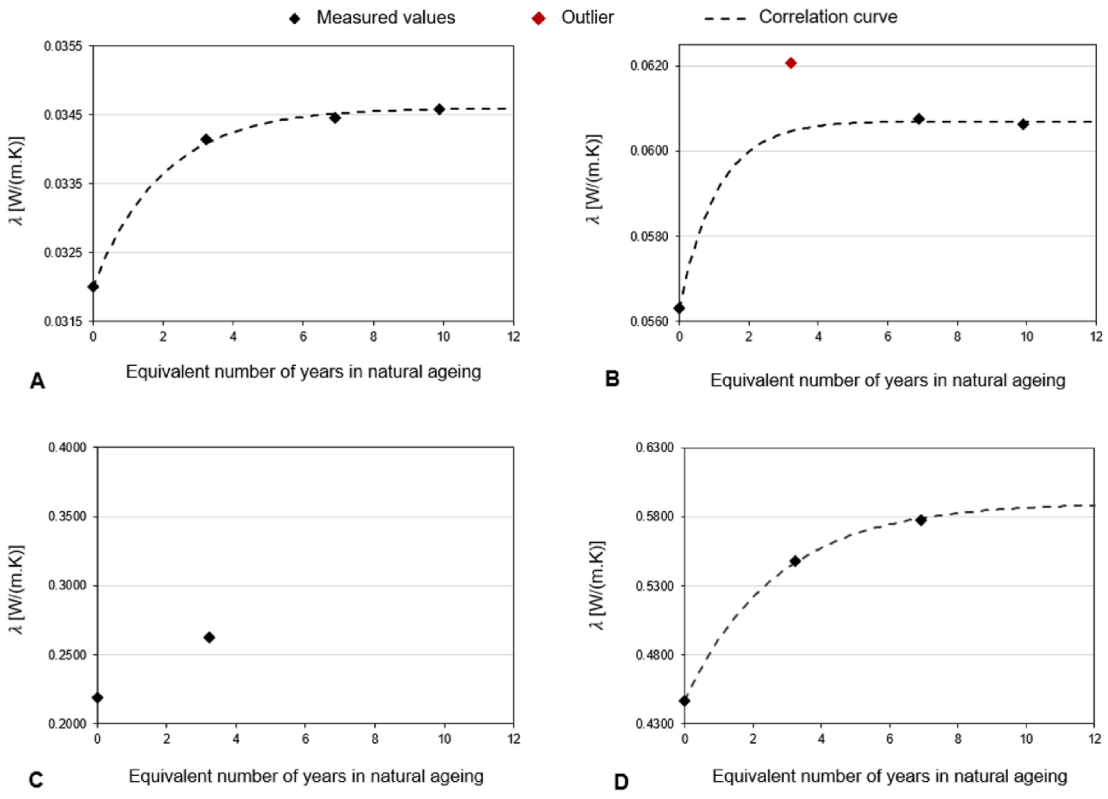

Fig. 6. Results of the long-term thermal conductivity during the elevated temperature ageing of mortars A^{AER} (A), B^{EPS} (B), C^{CORK} (C) and D^{REF} (D) (some values were not included in the models' due sample failure or inconsistency in the results).

Table 4
Parametric equations of the models of thermal conductivity trends of mortars during ageing in elevated temperature, high moisture and freeze–thaw cycles.

		Linear $\lambda = ay + \lambda_0$		Exponential (increasing) $\lambda = (\lambda_{lim} - \lambda_0)\left(1 - e^{-\frac{y}{\tau}}\right) + \lambda_0$			Exponential (decreasing) $\lambda = \lambda_{lim} - (\lambda_{lim} - \lambda_0)e^{-y/\tau}$			R^2
		a	λ_0	λ_0	λ_{lim}	τ	λ_0	λ_{lim}	τ	
Elevated temperature ageing	A^{AER}	–	–	0.0320	0.0346	2.0	–	–	–	0.998
	B^{EPS}	–	–	0.0563	0.0607	1.1	–	–	–	0.999[b]
	C^{CORK}	–	–	–	–	–	–	–	–	–[b,c]
	D^{REF}	–	–	0.4470	0.5900	2.7	–	–	–	0.999[b]
High moisture ageing	A^{AER}	–	–	0.0338	0.0374	2.8	–	–	–	0.999
	B^{EPS}	−0.0015	0.0540	–	–	–	–	–	–	0.986
	C^{CORK}	–	–	–	–	–	–	–	–	–[b,c]
	D^{REF}	0.0069	0.4146	–	–	–	–	–	–	0.934
Freeze-thaw cycles ageing	A^{AER}	–	–	0.0314	0.0340	2.2	–	–	–	0.999
	B^{EPS}	–	–	–	–	–	0.0523	0.0407	2.3	0.999
	C^{CORK}	–	–	0.1940	0.2168	5.3	–	–	–	0.999[b]
	D^{REF}	–	–	0.4121	0.5056	1.0	–	–	–	0.999[a,b]

[a]Some values were not included in the model due to the failure of the specimen; [b]Some values were not included in the model due to inconsistency of the results. [c]No meaningful correlation model could be found.

outlier due to a measurement error, it becomes feasible to correlate the remaining data points with an "increasing exponential" function (R^2 = 0.999) similar to the other mortars. In this case, the model shows a shorter characteristic degradation time (1.1 years), indicating a stabilisation of the loss of performance after around 3 years of ageing and yielding a long-term thermal conductivity value of 0.0607 W/(m.K) (i.e., 7.2 % higher compared to the unaged state). On the other hand, the brittle nature of C^{CORK} compromised the thermal conductivity measurements after 14 days of accelerated ageing in elevated temperature, thereby making it impossible to establish a meaningful trend.

4.2.3. Biological colonisation

Fig. 7A shows the average rate of mould growth obtained each week for the specimens aged in elevated temperature. Apart from D^{REF}, all the mortars showed signs of growth from the first week of testing.

The mortar A^{AER} was colonised at a constant rate (Fig. 8A,D). On the other hand, higher levels of mould growth were observed in mortar B^{EPS} since the beginning of the test (Fig. 8B). In fact, mortar B^{EPS} showed light mould growth (10 to 30 % of contaminated surface) after the second week of test, followed by a stabilisation after that period. Additionally, mortar C^{CORK} showed the highest susceptibility to mould growth after

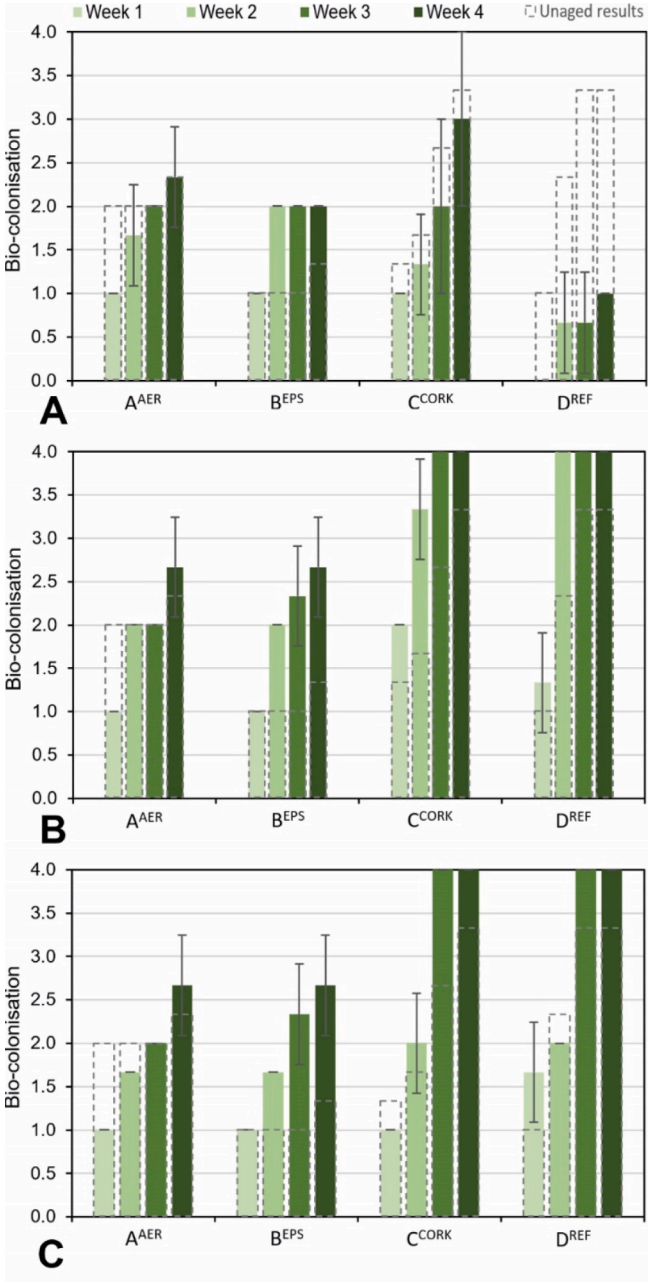

Fig. 7. Average results of mould growth on A^{AER}, B^{EPS}, C^{CORK} and D^{REF} samples after elevated temperature (A), high moisture (B) and freeze–thaw (C) ageing.

four weeks of testing. Conversely, mortar D^{REF} showed the lowest susceptibility to bio-colonisation, showing only traces of mould growth (<10 % of contaminated surface) at the end of the test (Fig. 8C,E).

4.3. High moisture ageing

4.3.1. Visual assessment

The experimentally designed mortars C^{CORK} and D^{REF} showed only few signs of degradation during the high moisture ageing procedure. The surface of B^{EPS} did not visibly change in appearance, and only localised marks were observed on A^{AER}. Indeed, after 21 days of ageing (i.e., ~ 3 years of natural ageing), a few isolated cracks (Fig. 5D) and a dark spot (Fig. 5E) that could be attributed to the development of mould were observed on the lower edge of the sample, in contact with the perforated metal grid. C^{CORK} showed signs of mechanical brittleness, as also observed at elevated temperature. Additionally, a piece of the upper part of the sample broke after 21 days of ageing. On the other hand, mortar D^{REF} presented signs of cohesion loss by crumbling, particularly at the corners of the sample (Fig. 5F).

4.3.2. Long-term thermal conductivity

Fig. 9 shows the trend of the thermal conductivity variation during the high moisture accelerated ageing.

Unlike what was observed in the elevated temperature ageing, the thermal conductivity of the mortars did not systematically increase. In fact, results showed that the thermal conductivity of mortar B^{EPS} significantly decreased after the high moisture ageing procedure, from 0.0546 W/(m.K) to 0.0394 W/(m.K), i.e., a decrease of ~28 %. This trend was not expected and could not be explained considering solely the visual observations and the thermal conductivity results. Considering that such results were not observed in elevated temperature ageing, during which the mortar samples were dried, this phenomenon may be attributed to interactions between water and the mortar's matrix. Previous studies have suggested that the presence of water could lead to the degradation and leaching of lime crystals [40–42], thereby increasing porosity and consequently decreasing the thermal conductivity of the mortar [43,44]. However, further tests, such as porosity measurements by mercury intrusion (MIP) or scanning electron microscope (SEM) observations, would be necessary to strengthen this hypothesis. Additionally, mortar A^{AER} showed similar behaviour to that observed after elevated temperature ageing. The thermal conductivity of this mortar increased between the unaged state and the first measurement (i.e., corresponding to ~3 years of natural ageing), with an increase from 0.0338 W/(m.K) to 0.0363 W/(m.K), and then reaching a thermal conductivity of 0.0373 W/(m.K) at the end of the ageing procedure. Similarly to the elevated temperature ageing, the thermal conductivity of mortar D^{REF} significantly increased from 0.419 W/(m.K) to 0.482 W/(m.K) after ~10 years of natural ageing, without any sign of stabilisation after the ageing procedure (Fig. 9D). After approximately 3 years of natural ageing, the first measurement of thermal conductivity in mortar C^{CORK} showed an increase of 2.7 % compared to the unaged state, showing a slight loss of thermal performance. However, subsequent measurements did not yield any usable results. In fact, the impossibility of applying the correction formula (see Sections 4.2.2 and 5.3.2) led to a greater dispersion of results probably linked to the influence of moisture in the readings.

As with the previous ageing procedure, A^{AER} showed a good correlation with an "increasing exponential" function ($R^2 = 0.999$), predicting a long-term thermal conductivity of 0.0374W/(m.K), i.e., 9.6 % higher compared to the unaged state, with most of the deterioration occurring in the first 8 years of ageing ($3\tau = 8.4$ years). For this ageing test, the trend followed by D^{REF} is closer to a linear evolution ($R^2 = 0.934$), with an increase in thermal conductivity of 6.9×10^{-3}[W/(m.K)]/year, i.e., a loss of performance of around 1.6 % per year. Conversely, the thermal conductivity of B^{EPS} decreased linearly ($R^2 = 0.986$), with a rate of -1.5×10^{-3}[W/(m.K)]/ year, representing a significant improvement in thermal performance of 2.7 % per year. Despite being strongly correlated with experimental results, these models cannot be used to forecast long-term thermal conductivity, since they predict an indefinitely constant variation. However, this may indicate that the degradation mechanisms take place over a longer period of time, and that an observation period of 10 years is not sufficient to define long-term trends. Therefore, for these mortars, the data available merely suggests a linear variation in thermal conductivity in the first decade after application, with no quantified indication of duration of the stabilisation phase. Finally, no model was selected to describe the evolution of C^{CORK}, as the number of usable measurements was limited.

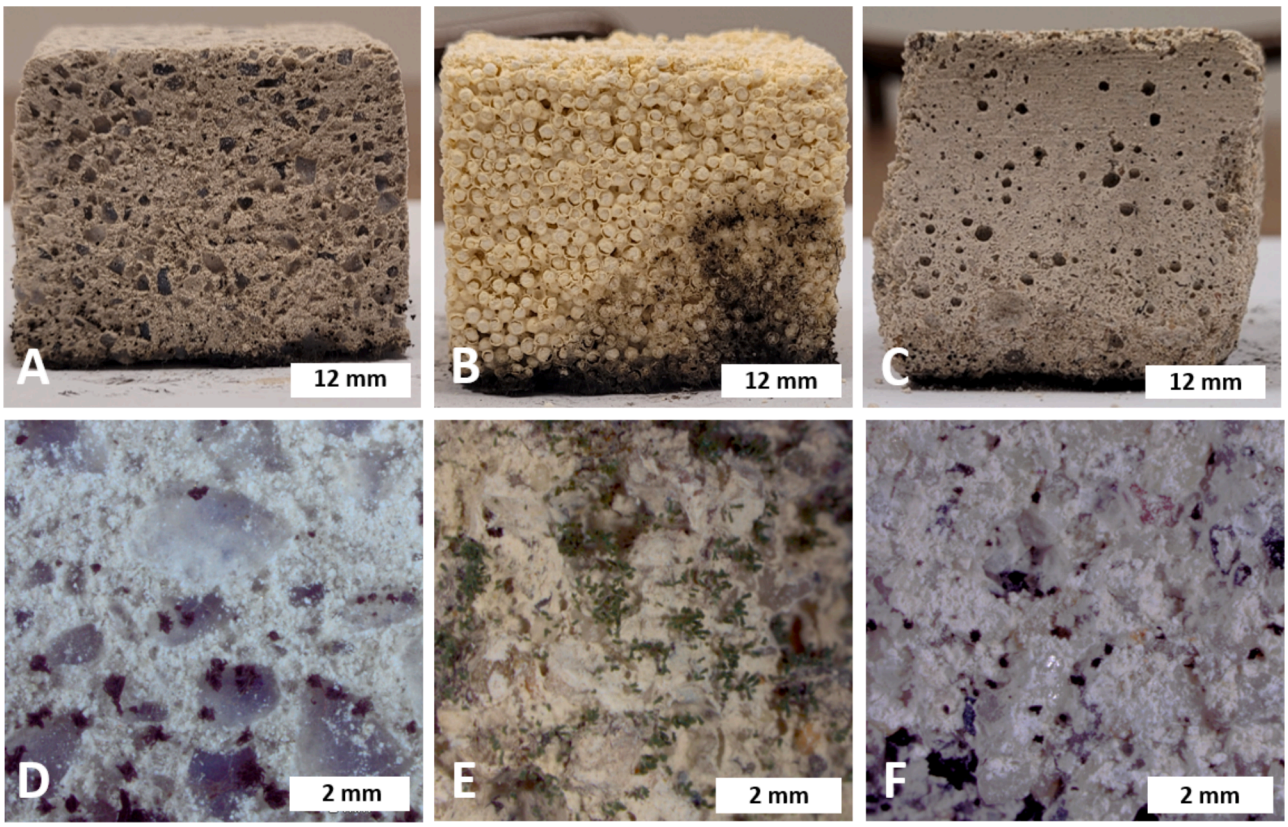

Fig. 8. Visual observations of the elevated temperature-aged mortars after the biological colonisation tests: A^{AER} (A); B^{EPS} (B); D^{REF} (C) and stereomicroscope images: A^{AER} (D); C^{CORK} (E); D^{REF} (F).

4.3.3. Biological colonisation

The average rate of biological colonisation for mortars aged in a high moisture environment is shown in Fig. 7B. All aged mortars proved to be more susceptible to bio-colonisation when compared to the unaged state. This difference was particularly noted for B^{EPS}, showing light mould growth after the second week of testing (Fig. 10A). Numerous water droplets were also observed in this mortar, indicating significant surface condensation during the test (Fig. 10D). The same phenomenon was also identified in the case of the mortar with silica aerogel aggregates (A^{AER}). Additionally, both C^{CORK} and D^{REF} mortars proved to be highly susceptible to biological colonisation (Fig. 10B,C,E,F), showing heavy mould growth (i.e., more than 60 % of contaminated surface) after 3 weeks of testing.

4.4. Freeze-thaw ageing

4.4.1. Visual assessment

As with the other ageing procedures, mortar C^{CORK} presented a brittle behaviour, and broke at two-thirds of its height during handling before the measurements began. The thermal conductivity measurements were therefore carried out on the bigger part, whose dimensions (approximately 200 mm × 300 mm × 50 mm) were sufficient to perform the heat flow measurements with the Holometrix rapid-K equipment. Furthermore, some brown spots were observed on the surface of this sample during the ageing procedure, possibly indicating some depigmentation of the cork aggregates (Fig. 5G). The surface of the mortar D^{REF} was significantly affected after ageing, with the appearance of grey spots and defacements (Fig. 5H). After 8 days of freeze–thaw ageing (i.e., approximately 6 years of natural ageing), a corner of D^{REF} cracked and detached during a freezing phase (Fig. 5I). No visible signs of degradation were observed on mortars A^{AER} and B^{EPS}.

4.4.2. Long-term thermal conductivity

Fig. 11 shows the trend of the thermal conductivity variation during the freeze–thaw accelerated ageing.

With the exception of mortar B^{EPS}, the thermal conductivity increased with ageing. The thermal performance of A^{AER} followed a non-linear trend similar to that observed in the elevated temperature ageing, with a significant increase in thermal conductivity after approximately 4 years of natural ageing (i.e., from 0.0314 W/(m.K) to 0.0335 W/(m.K)), followed by a slight increment reaching 0.0339 W/(m.K) after 10 years of natural ageing). On the other hand, mortar B^{EPS} showed an opposite trend, with a significant decrease in thermal conductivity in the first few years of ageing, achieving 0.0431 W/(m.K) after 4 years and 0.0408 W/(m.K) at the end of the procedure, corresponding to 10 years of natural aging. The thermal performance of mortar C^{CORK} increased from 0.194 W/(m.K) to 0.214 W/(m.K) after approximately 10 years of natural ageing, corresponding to ~10 % increase. Furthermore, a significant increase of thermal conductivity was also obtained for mortar D^{REF} (from 0.412 W/(m.K) to 0.505 W/(m.K)), followed by a stabilisation after 4 years of natural ageing. It is worth noting, however, that the fact that C^{CORK} and D^{REF} mortars failed during the ageing procedure made it impossible to apply the correction equations to all the measurements (see Section 3.3.2). In addition, some inconsistent values (i.e., 4-year measurement for C^{CORK} and 10-year measurement for D^{REF}) were removed from the models.

The thermal conductivity results obtained for mortars A^{AER}, C^{CORK} and D^{REF} show in all three cases a strong exponential correlation with natural ageing time ($R^2 > 0.93$) (Table 4). In accordance with the results obtained in the elevated temperature ageing, mortar A^{AER} showed only a ~8 % increase of thermal conductivity (limit value) after freeze–thaw ageing, with a characteristic degradation time of 2.2 years indicating that thermal conductivity will be mainly affected in the first 7 years of ageing. Considering the C^{CORK} mortar, a stabilisation in thermal

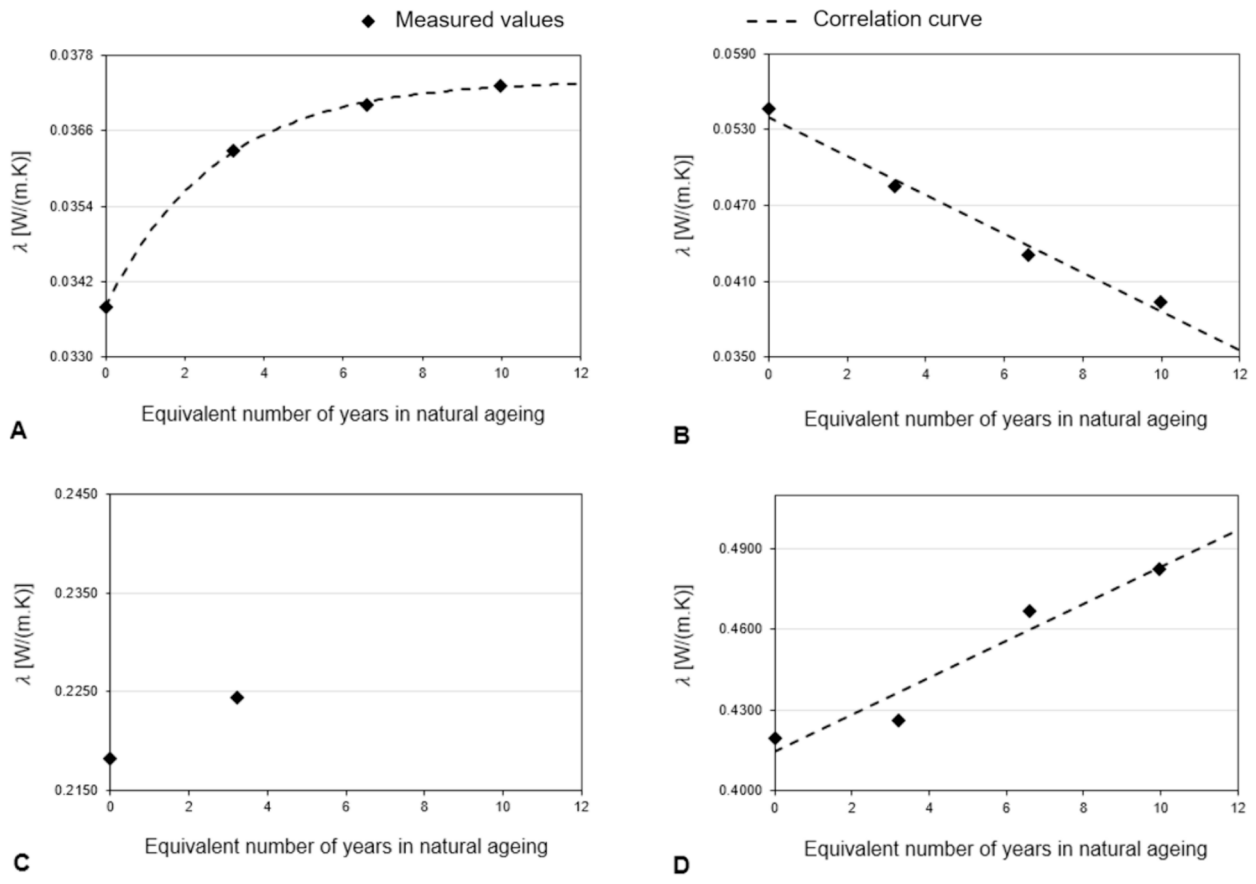

Fig. 9. Results of the long-term thermal conductivity during the high moisture ageing of mortars A^{AER} (A), B^{EPS} (B), and C^{CORK} (C) and D^{REF} (D) (some values were not included in the models' due sample failure or inconsistency in the results).

conductivity (i.e., a total variation lower than 5 %) is achieved after approximately 16 years of natural ageing, showing a characteristic degradation time of 5.3 years (Table 4). Nevertheless, the limit value is 11.7 % higher if compared to the initial state (unaged conditions), showing a moderate influence of the freeze–thaw ageing on the thermal performance of this mortar. Conversely, the thermal conductivity of D^{REF} underwent a fast and significant increase under freeze–thaw, with ~22 % increase (from 0.412 W/(m.K) to 0.501 W/(m.K)) registered after 3 years of natural ageing, and then stabilising with a long-term thermal conductivity about 22.7 % higher when compared to unaged conditions. Finally, the trend observed for B^{EPS} is noticeably different, showing an exponential negative variation of thermal conductivity with ageing time ($R^2 = 0.999$) (Fig. 11B; Table 4). Indeed, it is possible to observe that the thermal performance of this mortar significantly improves in the first years of ageing, and then tends to stabilise towards a limit value estimated at 0.0407 W/(m.K), which is ~ 29 % lower than that measured in the initial state. Similarly to the case of high moisture ageing, this enhancement in thermal performance may result from an increase of porosity within the mortar matrix.

4.4.3. *Biological colonisation*

Fig. 7C shows the results of the biological colonisation tests on the samples after freeze–thaw ageing. As with the other tests, all mortars proved to be susceptible to bio-colonisation. In fact, all mortars showed significantly higher levels of mould growth compared to the unaged state, after the second week of exposure (Fig. 7C).

Mortar A^{AER} was progressively colonised, presenting light mould growth (10 to 30 % of contaminated surface) after the third week of testing. Additionally, slight traces of mould were also observed in this mortar (Fig. 12D), retaining some drops of condensation water in some cases. B^{EPS} mortar samples showed light mould growth after three weeks of testing (Fig. 12**B**). On the other hand, the level of bio-colonisation on mortars C^{CORK} and D^{REF} was considerably higher, with all samples rated 4 out of 4 (i.e., heavy growth – more than 60 % of contaminated surface) after three weeks of testing.

5. Discussion

Visual observations of the samples during the different ageing procedures revealed that the experimentally designed mortars showed greater signs of visible deterioration compared to the industrially produced mortars. Indeed, both mortars C^{CORK} and D^{REF} have been subject to surface defacement, matrix crumbling and the appearance of stains. More importantly, C^{CORK} fractured during all the ageing procedures, showing mechanical properties that were too low for practical uses. This behaviour can be explained in part by the absence of admixtures in the formulation, which would have been necessary to compensate for the drop in the mixture's mechanical properties due to the incorporation of lightweight aggregates [30]. Considering the freeze–thaw ageing, D^{REF} also broke, probably due to the strong internal stresses induced by the contraction and dilation of the material and by the expansion of water when freezing. B^{EPS} only showed signs of degradation during the elevated temperature ageing, when the agglomerates of EPS beads appeared on the surface of the mortar. This can be explained by the plasticisation of the polystyrene [45] under the effect of temperature, leading to its deformation. As for A^{AER}, only slight marks of degradation were locally observed after high moisture ageing.

Fig. 13 shows the relative variations in the thermal conductivity of the mortars tested during the three accelerated ageing procedures.

The industrially produced mortars showed an overall improved

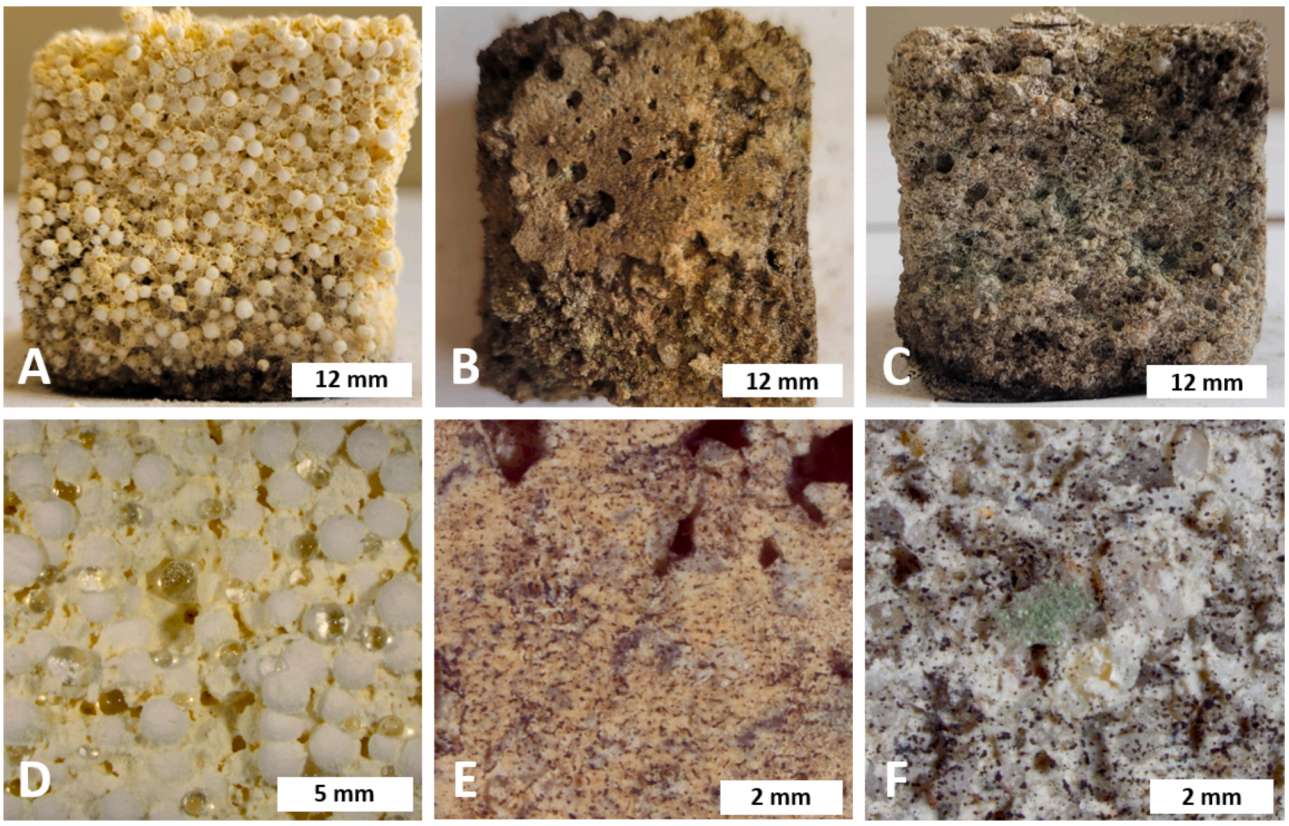

Fig. 10. Visual observations of the high moisture-aged mortars after the biological colonisation tests: B^{EPS} (A); C^{CORK} (B); D^{REF} (C) and stereomicroscope images: B^{EPS} (D); C^{CORK} (E); D^{REF} (F).

ageing performance when compared to the mortars designed in the laboratory, although with remarkably different trends. The thermal conductivity of A^{AER} did not increase by more than 10 %, regardless of the type of ageing (Fig. 13). It can thus be concluded that this mortar retains a good thermal performance after ageing, if compared to commonly used thermal insulation materials in unaged conditions (e.g., EPS boards, with a thermal conductivity of ~0.0370 W/(m.K) [46]). On the other hand, B^{EPS} only showed a loss of performance in elevated temperature ageing, with a maximum increase of 10 % of thermal conductivity (Fig. 13), which was possibly related to the previously observed degradation of the aggregates. For the other ageing procedures, the thermal conductivity of this mortar followed a significant downward trend, falling by up to 28 % (Fig. 13).

In order to find an explanation to this unexpected behaviour, Scanning Electron Microscopy (SEM) analysis was performed in these samples using a TESCAN MIRA 3-field emission microscope combined with a BRUKER XFlash 6|30 EDS system. Prior to the analysis, all B^{EPS} samples were sputtered with an Au film. The observations were made in backscattered electrons mode (BSE) at an accelerating voltage of 20 kV with the samples at a working distance of 14 ± 1 mm. Fig. 14 shows the SEM images of the reference samples (Fig. 14A,C) and of samples aged under high moisture conditions (Fig. 14B,D). It can be observed the presence of crystals in the form of plates identified as calcium hydroxide (CH) (Fig. 14A,B) in the matrix of the mortar, thus suggesting the use of lime in its formulation. Fine needle-shaped crystals were also observed (Fig. 14D) and identified as calcium silicate hydrate (CSH), also indicating the use of a hydraulic binder (hydraulic lime or Portland cement) in the formulation. When comparing Fig. 14A,C with Fig. 14B,D, a decrease in the presence of CH and CSH crystals after ageing can be observed, possibly leading to a reduced compactness of the mortar. Moreover, the presence of water in the high moisture test may have favoured the dissolution and leaching of some CH and CSH crystals [26,40–42], locally reducing the cohesion of the matrix and thus leading to the appearance of additional macropores [42] as a result of granular disintegration [26,40]. Subsequent tests performed in the unaged and aged mortars showed an increase in the capillary water absorption coefficient and a decrease in the compressive strength after ageing, thus supporting the hypothesis of an increase in mortar porosity [4,41–43,47]. For the mortars submitted to freeze–thaw ageing, a similar phenomenon might have occurred, although to a lesser extent, during the cooling period and possibly leading to surface condensation in the mortar. The temperature variation in the ageing procedure may also have had an influence on the results, by causing cracks and an increase of porosity [48]. Considering that several previous studies (e.g., [43,44]) reported a significant correlation between porosity and thermal conductivity, an increase in the porosity of B^{EPS} mortars after ageing can explain the decrease of thermal conductivity.

The failure of the C^{CORK} mortar compromised a number of thermal conductivity measurements, and therefore the results obtained in this case are less comprehensive than for the other mortars. Nevertheless, the available data suggest that the elevated temperature procedure was the most severe, considering that it caused an increase of ~20 % in thermal conductivity after three years of natural ageing (Fig. 13). A similar performance was also observed for D^{REF}, whereas the industrially produced mortars proved to be much more durable with respect to this type of ageing. It is thus probable that the addition of cork did not have a major influence on this result, and that the main factor in improving resistance to high temperatures was the optimisation of the formulation of the industrially produced mortars using admixtures. Regarding freeze–thaw ageing, C^{CORK} mortar showed a significantly lower increase in thermal conductivity than D^{REF} (+10 % compared with +23 % over 10 years) (Fig. 13). This may be linked to the addition of cork aggregates, which increased the deformability of the mortar [30] and could have limited the stresses induced by volume variations caused by

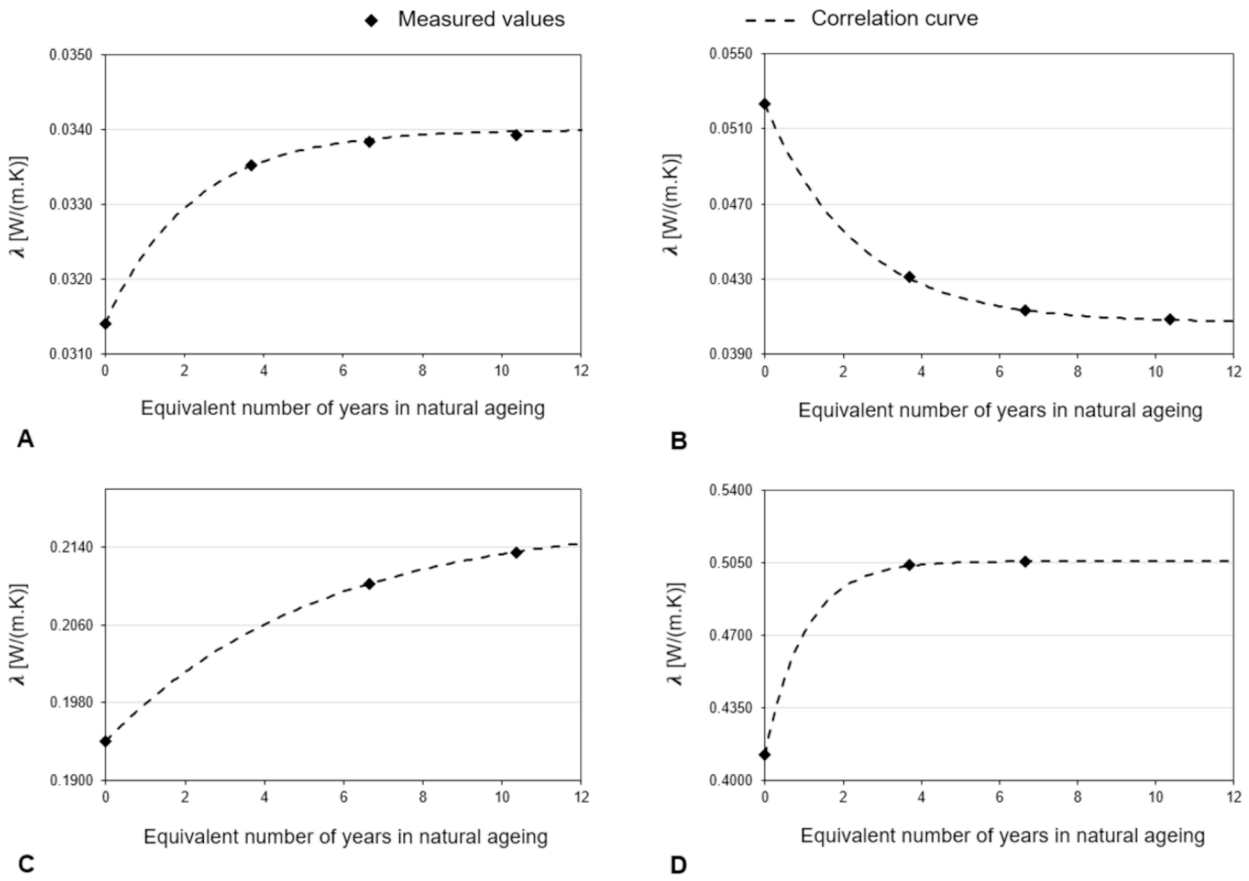

Fig. 11. Results of the long-term thermal conductivity during the freeze–thaw ageing of mortars A^{AER} (A), B^{EPS} (B), C^{CORK} (C) and D^{REF} (D) (some values were not included in the models' due to sample failure or inconsistency in the results).

temperature variations. The results obtained for D^{REF} during high moisture ageing revealed that this mortar degraded over a significatively longer time than industrial mortars. In fact, a linear increase in thermal conductivity without stabilisation was measured over the duration of the test, suggesting that this mortar would have continued to degrade over a longer period of time. This difference in behaviour could be related to the fact that this mortar, which was much denser compared to the others, absorbed water over a longer period of time, thus delaying the degradation mechanisms.

All the mortars tested proved to be susceptible to biological colonisation, regardless of the ageing procedure. The samples subjected to the high moisture ageing were, however, significantly more susceptible to this anomaly. Since many studies have reported a strong link between moisture content and biological colonisation (e.g., [49,50]), it is possible that this result is due to the fact that the samples retained more water after being exposed to high humidity levels, thus favouring mould growth. The difference between the growth rates obtained for the unaged samples and those aged by high moisture was particularly marked in the case of B^{EPS}, whose porosity and capillary absorption coefficient increased after ageing. This may have favoured the absorption of water by the mortar during the bio-colonisation test and therefore increased its bio-susceptibility. Conversely, the elevated temperature ageing procedure had the least influence on the mould growth results, and even led to a decrease in the colonisation rate of the experimentally produced mortars C^{CORK} and D^{REF} in comparison with the unaged samples. In particular, D^{REF} showed only very slight traces of mould growth after ageing. This can be explained by the large quantity of lime used in its formulation, which gave a highly alkaline nature to its matrix, inhibiting mould growth, whose ideal development conditions usually require slightly acidic pH levels [51,52]. Finally, freeze–thaw ageing moderately increased the biological susceptibility of the mortars. In fact, this type of ageing is conducive to the appearance of microcracks and to increase both surface roughness and open porosity of mortars, which are factors known to favour mould growth [53]. Indeed, results showed that the rougher surfaces of the experimentally designed mortars after freeze–thaw ageing considerably affected biological colonisation.

Overall, results showed that A^{AER} and B^{EPS} industrial mortars were less susceptible to biological colonisation compared to the experimentally designed C^{CORK} and D^{REF} mortars. The physical properties of the mortars may explain the difference. In fact, mortars A^{AER} and B^{EPS} have hydrophobic surfaces due to the nature of the aggregates incorporated, lower capillary water absorption coefficients and greater water vapour permeability compared to C^{CORK} and D^{REF} mortars, which minimise the risk of moisture accumulation. In addition, the particularly marked degradation of the experimental mortars' matrix provided an overall rougher surface compared to the industrially produced mortars, a factor that can also favour mould growth [53].

6. Conclusions

With the aim of assessing the long-term thermal conductivity and the susceptibility to biological colonisation of thermal insulating mortars incorporating EPS, cork and silica aerogel aggregates, artificial ageing procedures were used in order to accelerate the degradation mechanisms. The long-term performance of the mortars was assessed prior, during and after exposure to three accelerated ageing tests including elevated temperature, freeze–thaw cycles and high humidity levels. The following conclusions can be drawn:

- The industrially produced mortars A^{AER} and B^{EPS} showed significantly enhanced thermal performance when compared to the

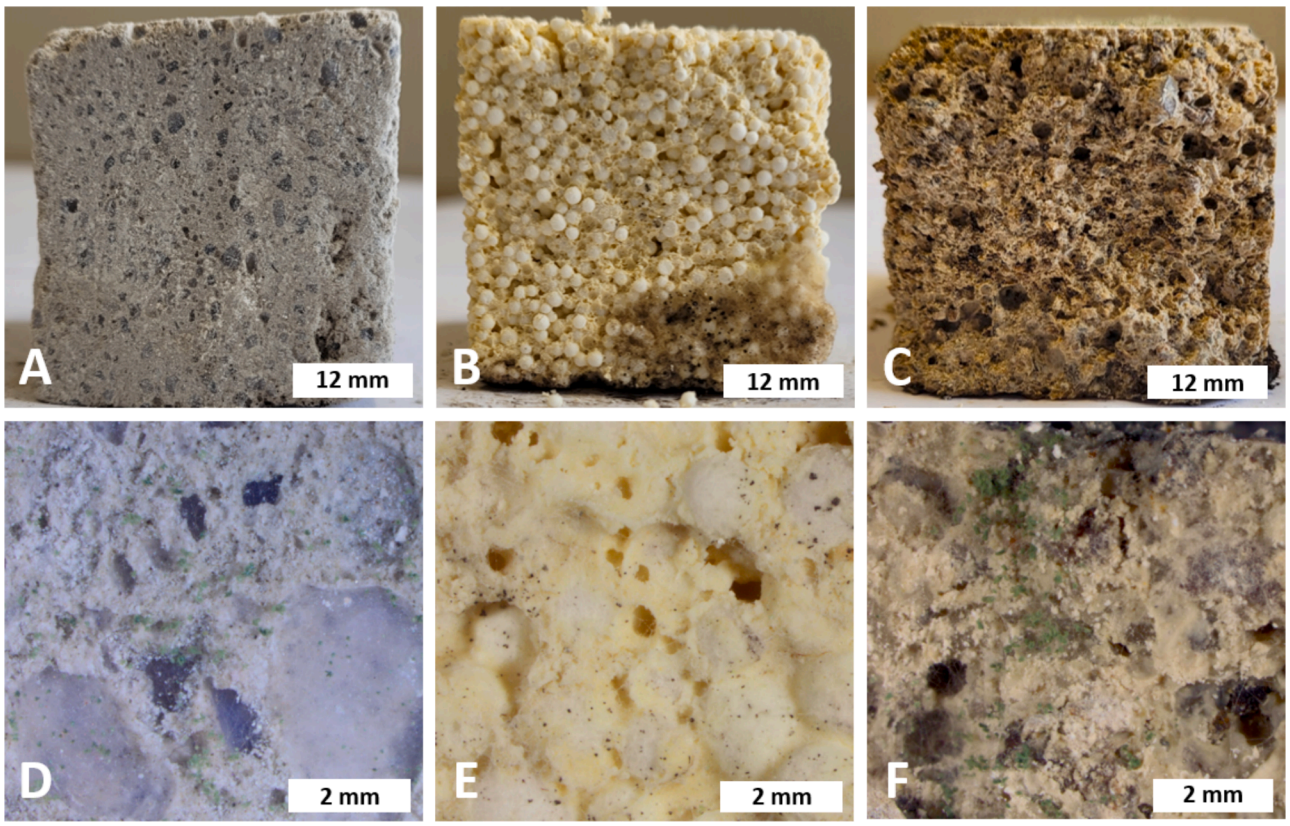

Fig. 12. Visual observations of the freeze–thaw cycles-aged mortars after the biological colonisation tests: A^{AER} (A); B^{EPS} (B); C^{CORK} (C) and stereomicroscope images: A^{AER} (D); B^{EPS} (E); C^{CORK} (F).

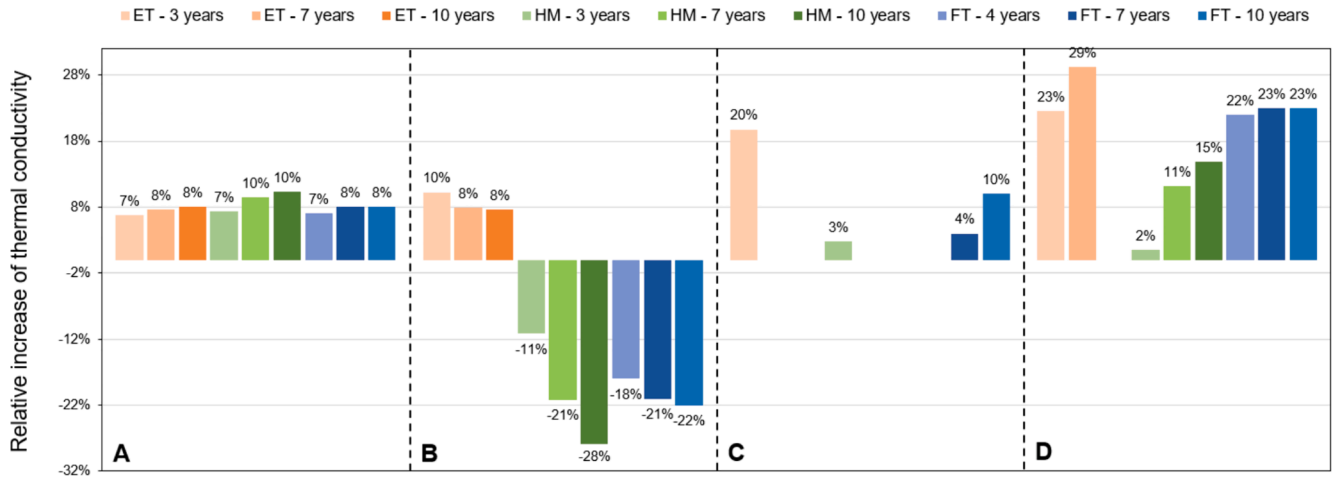

Fig. 13. Relative variations in thermal conductivity of mortars A^{AER} (A), B^{EPS} (B), C^{CORK} (C) and D^{REF} (D) during elevated temperature (ET), high moisture (HM) and freeze–thaw (FT) ageing.

experimentally designed mortars C^{CORK} and D^{REF} probably due a more optimised formulation of the industrialized ones. Nevertheless, the addition of cork aggregates resulted in a significant improvement in the performance of C^{CORK} compared to D^{REF}.

- Industrially produced mortars proved to have a good durability considering the evolution of their thermal conductivity throughout the ageing procedures, which did not increase by more than 10 % after accelerated ageing (corresponding to 10 years of exposure to natural weather conditions). On the other hand, thermal conductivity increased more than 20 % after ageing for the experimentally designed mortars.
- Elevated temperature was the most damaging degradation agent for all mortars, except for the thermal mortar with silica aerogel aggregates A^{AER}, for which the high moisture test was more severe.
- A significant reduction in the thermal conductivity of mortar B^{EPS} was observed after high moisture (maximum decrease of 28 %) and freeze–thaw (maximum decrease of 22 %) ageing.
- All the mortars proved to be susceptible to biological colonisation, with the greatest values of mould growth obtained after the high moisture content ageing for the experimentally designed mortars.

In this study, the durability of the mortars was assessed using a

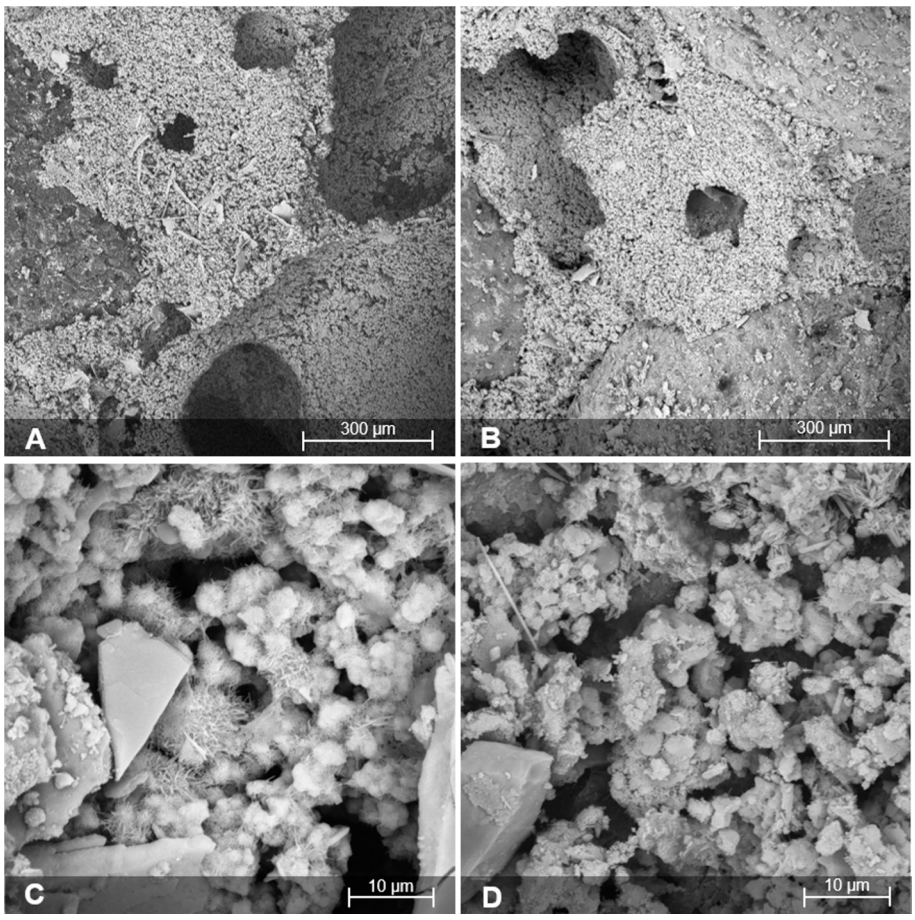

Fig. 14. SEM images of mortar B^{EPS} in the unaged state (A,C) and after high moisture ageing (B,D).

performance-based approach, which consisted of evaluating differences in a set of properties during three accelerated ageing procedures. This method provides a good indication on the long-term performance of the mortars; however, it does not offer a comprehensive depiction of all degradation mechanisms involved, thus limiting the interpretation of the results. Additional research investigating the physical and chemical-morphological aspects related to these mechanisms would complement the present study and provide a better understanding of the long-term performance of thermal insulating mortars.

CRediT authorship contribution statement

Léo Pinchard: Writing – original draft, Visualization, Validation, Methodology, Investigation, Formal analysis, Data curation. **João L. Parracha:** Writing – original draft, Validation, Project administration, Methodology, Investigation, Conceptualization. **Rosário Veiga:** Writing – review & editing, Supervision, Resources, Project administration, Methodology, Funding acquisition, Conceptualization. **Luís Matias:** Writing – review & editing, Supervision, Resources, Project administration, Methodology. **António Santos Silva:** Writing – review & editing, Resources, Investigation, Formal analysis. **Sónia Duarte:** Writing – review & editing, Validation, Investigation, Formal analysis. **Lina Nunes:** Writing – review & editing, Resources.

Declaration of competing interest

The authors declare that they have no known competing financial interests or personal relationships that could have appeared to influence the work reported in this paper.

Data availability

Data will be made available on request.

Acknowledgements

The authors acknowledge LNEC research projects “REuSE – Coatings for rehabilitation: safety and sustainability” and “ConstBio – Development and optimisation of biomaterials for construction” and Marta Duarte (LNEC) for the help in the biological colonisation tests. Saint-Gobain and Secil are also acknowledged for the material supply. The Portuguese Institute for Sea and Atmosphere (IPMA) is acknowledged for the meteorological data.

Appendix A. Supplementary data

Supplementary data to this article can be found online at https://doi.org/10.1016/j.enbuild.2024.114403.

References

[1] United Nations, “Climate change: An ‘existential threat’ to humanity, UN chief warns global summit.” Accessed: Apr. 20, 2023. [Online]. Available: https://news.un.org/en/story/2018/05/1009782.
[2] European Commission, “2050 long-term strategy.” Accessed: Apr. 20, 2023. [Online]. Available: https://climate.ec.europa.eu/eu-action/climate-strategies-targets/2050-long-term-strategy_en.
[3] European Commission, “Energy performance of buildings directive.” Accessed: Apr. 20, 2023. [Online]. Available: https://energy.ec.europa.eu/topics/energy-efficiency/energy-efficient-buildings/energy-performance-buildings-directive_en.
[4] P.F. Bergmann Becker, C. Effting, A. Schackow, Lightweight thermal insulating coating mortars with aerogel, EPS, and vermiculite for energy conservation in

buildings, Cem. Concr. Compos. 125 (2022), https://doi.org/10.1016/j.cemconcomp.2021.104283.
[5] M.G. Gomes, I. Flores-Colen, F. da Silva, M. Pedroso, Thermal conductivity measurement of thermal insulating mortars with EPS and silica aerogel by steady-state and transient methods, Constr. Build. Mater. 172 (2018) 696–705, https://doi.org/10.1016/j.conbuildmat.2018.03.162.
[6] M.G. Gomes, I. Flores-Colen, H. Melo, A. Soares, Physical performance of industrial and EPS and cork experimental thermal insulation renders, Constr. Build. Mater. 198 (2019) 786–795, https://doi.org/10.1016/j.conbuildmat.2018.11.151.
[7] J. Maia, N.M.M. Ramos, R. Veiga, Assessment of test methods for the durability of thermal mortars exposure to freezing, Mater. Struct. 52 (6) (2019), https://doi.org/10.1617/s11527-019-1411-4.
[8] J.L. Parracha, A.R. Santos, R. Lazera, I. Flores-Colen, M.G. Gomes, A.M. Rodrigues, Performance of lightweight thermal insulating mortars applied on brick substrate specimens and prototype wall, Constr. Build. Mater. 364 (2023), https://doi.org/10.1016/j.conbuildmat.2022.129954.
[9] A. Brás, M. Leal, P. Faria, Cement-cork mortars for thermal bridges correction. Comparison with cement-EPS mortars performance, Constr. Build. Mater. 49 (2013) 315–327, https://doi.org/10.1016/j.conbuildmat.2013.08.006.
[10] U. Berardi, R.H. Nosrati, Long-term thermal conductivity of aerogel-enhanced insulating materials under different laboratory aging conditions, Energy 147 (2018) 1188–1202, https://doi.org/10.1016/j.energy.2018.01.053.
[11] M. Pedroso, I. Flores-Colen, J.D. Silvestre, M.G. Gomes, L. Silva, L. Ilharco, Physical, mechanical, and microstructural characterisation of an innovative thermal insulating render incorporating silica aerogel, Energy Build. 211 (2020), https://doi.org/10.1016/j.enbuild.2020.109793.
[12] M. Vyšvařil, et al., Non-hydrophobized perlite renders for repair and thermal insulation purposes: Influence of different binders on their properties and durability, Constr. Build. Mater. 263 (2020) 120617, https://doi.org/10.1016/j.conbuildmat.2020.120617.
[13] Z. Pavlík, M. Pavlíková, M. Záleská, M. Vyšvařil, T. Žižlavský, Lightweight thermal efficient repair mortars with expanded glass (EG) for repairing historical buildings: The effect of binder type and EG aggregate dosage on their performance, Energy Build. 276 (2022) 112526, https://doi.org/10.1016/j.enbuild.2022.112526.
[14] EN 998-1:2017 - European Committee for Standardization, "Specification for mortar for masonry - Part 1: Rendering and plastering mortar," 2017.
[15] M. Posani, R. Veiga, V.P. de Freitas, Retrofitting historic walls: Feasibility of thermal insulation and suitability of thermal mortars, Heritage 4 (3) (2021) 2009–2022, https://doi.org/10.3390/HERITAGE4030114.
[16] M. Posani, R. Veiga, V.P. de Freitas, Thermal mortar-based insulation solutions for historic walls: An extensive hygrothermal characterization of materials and systems, Constr. Build. Mater. 315 (2022), https://doi.org/10.1016/j.conbuildmat.2021.125640.
[17] A.R. Santos, M.do R. Veiga, A. Santos Silva, Characterization and assessment of performance of innovative lime mortars for conservation of building heritage: Paimogo's fort, a case study, Appl. Sci. 13 (8) (2023) 4679, https://doi.org/10.3390/app13084679.
[18] Th. Stahl, S. Brunner, M. Zimmermann, K.G. Wakili, Thermo-hygric properties of a newly developed aerogel based insulation rendering for both exterior and interior applications, Energy Build. 44 (2012) 114–117, https://doi.org/10.1016/j.enbuild.2011.09.041.
[19] Á. Lakatos, Investigation of the thermal insulation performance of fibrous aerogel samples under various hygrothermal environment: Laboratory tests completed with calculations and theory, EnergyBuild. 214 (2020) 109902, https://doi.org/10.1016/j.enbuild.2020.109902.
[20] R.H. Nosrati, U. Berardi, Hygrothermal characteristics of aerogel-enhanced insulating materials under different humidity and temperature conditions, Energy Build. 158 (2018) 698–711, https://doi.org/10.1016/j.enbuild.2017.09.079.
[21] Z. Kovács, A. Csík, Á. Lakatos, Thermal stability investigations of different aerogel insulation materials at elevated temperature, Therm. Sci. Eng. Prog. 42 (2023) 101906, https://doi.org/10.1016/j.tsep.2023.101906.
[22] Á. Lakatos, Stability investigations of the thermal insulating performance of aerogel blanket, Energy Build. 185 (2019) 103–111, https://doi.org/10.1016/j.enbuild.2018.12.029.
[23] J.L. Parracha, et al., Effects of hygrothermal, UV and SO_2 accelerated ageing on the durability of ETICS in urban environments, Build. Environ. 204 (2021), https://doi.org/10.1016/j.buildenv.2021.108151.
[24] L. Addelson. Buildings failures: A Guide to Diagnosis, Remedy and Prevention, third ed., Butterworth Architecture, Michigan, 1982.
[25] E. Barreira, V.P. de Freitas, Experimental study of the hygrothermal behaviour of external thermal insulation composite systems (ETICS), Build. Environ. 63 (2013) 31–39, https://doi.org/10.1016/J.BUILDENV.2013.02.001.
[26] S. Pavía, E. Treacy, A comparative study of the durability and behaviour of fat lime and feebly-hydraulic lime mortars, Mater. Struct. 39 (3) (2006) 391–398, https://doi.org/10.1617/s11527-005-9033-4.
[27] J.L. Parracha, et al., Performance parameters of ETICS: Correlating water resistance, bio-susceptibility and surface properties, Constr. Build. Mater. 272 (2021), https://doi.org/10.1016/j.conbuildmat.2020.121956.
[28] B.P. Jelle, Accelerated Climate Ageing of Building Materials, Components and Structures in the Laboratory, J. Mater. Sci. 47 (2012) 6475–6496, https://doi.org/10.1007/s10853-012-6349-7.
[29] Enersens, "Product datasheet: Aerogel kwark." 2015.
[30] L. Pinchard, J. Parracha, R. Veiga, L. Matias, and L. Nunes, "Assessment of the durability and sustainability of thermal mortars," Sep. 2023. Technical Report.
[31] EN 1097-3:1999 European Committee for Standardization, "Tests for mechanicaland physical properties of aggregates - Part 3: Determination of loose bulk density and voids." Brussels, Oct. 1999.
[32] S. Peck, Comprehensive model for humidity testing correlation. In: 24th International Reliability Physics Symposium, 01-03 April 1986, Anaheim, USA. doi: https://doi.org/10.1109/IRPS.21986.362110.
[33] L.A. Escobar, W.Q. Meeker, A review of accelerated test models, Stat. Sci. 21 (4) (2006) 552–577, https://doi.org/10.1214/088342306000000321.
[34] K.J. Laidler, The development of the Arrhenius equation, J. Chem. Educ. 61 (6) (1984) 494–498, https://doi.org/10.1021/ed061p494.
[35] EAD 040427-00-0404, Kits for external thermal insulation composite system (ETICS) with mortar as thermal insulation product and renderings or discontinuous claddings as exterior skin, in: Guideline for European Technical Approval, EOTA - European Organisation for Technical Approval, 2019.
[36] EN 12667:2001 European Committee for Standardization, "Thermal performance of building materials and products. Determination of thermal resistance by means of guarded hot plate and heat flow meter methods. Products of high and medium thermal resistance." 2001.
[37] EN 1602:2013 European Committee for Standardization, "Thermal insulating products for building applications - Determination of the apparent density." 2013.
[38] ISO 10456:2007 International Organization for Standardization, "Building materials and products — Hygrothermal properties — Tabulated design values and procedures for determining declared and design thermal values." 2007.
[39] ASTM D5590–17, Determining the Resistance of Paint Films and Related Coatings to Fungal Defacement by Accelerated Four-Week Agar Plate Assay, ASTM International, Pennsylvania, USA, 2021.
[40] R. Veiga, Air lime mortars: What else do we need to know to apply them in conservation and rehabilitation interventions? A review, Constr. Build. Mater. 157 (2017) 132–140, https://doi.org/10.1016/j.conbuildmat.2017.09.080. Elsevier Ltd.
[41] F.-J. Ulm, E. Lemarchand, F.H. Heukamp, Elements of chemomechanics of calcium leaching of cement-based materials at different scales, Engineering Fracture Mechanics 70 (2003) 7–8, https://doi.org/10.1016/S0013-7944(02)00155-8.
[42] C. Carde, R. François, J.-M. Torrenti, Leaching of both calcium hydroxide and C-S-H from cement paste: Modelling the mechanical behavior, Cem. Concr. Res. 26 (8) (1996) pp.
[43] F. Koksal, E. Mutluay, O. Gencel, Characteristics of isolation mortars produced with expanded vermiculite and waste expanded polystyrene, Constr. Build. Mater. 236 (2020).
[44] P. Shafigh, I. Asadi, A.R. Akhiani, N.B. Mahyuddin, M. Hashemi, Thermal properties of cement mortar with different mixproportions, Materiales De Construccion 70 (339) (2020), https://doi.org/10.3989/mc.2020.09219.
[45] INRS : Santé et Sécurité au travail, "Plastiques, Risque et Analyse ThermIQue Polystyrène PS Présentation du polymère Synthèse Formule développée n°1 Caractéristiques Propriétés physico-chimiques." [Online]. Available: http://www.inrs.fr/publications/bdd/fichetox/fiche.html?refINRS=FICHETOX_3.
[46] SINIAT, "Technical data sheet: 'GTEC Thermal EPS Board,'" 2013.
[47] J. Thamboo, N. Jayarathne, A. Bandara, Characterisation and mix specification of commonly used masonry mortars, SN Appl. Sci. 1 (4) (2019), https://doi.org/10.1007/s42452-019-0312-z.
[48] J. Fernandes Maia, "DURABILITY OF THERMAL RENDERING AND PLASTERING SYSTEMS," 2019. [Online]. Available: http://www.fe.up.pt.
[49] S. Ximenes, J. de Brito, P.L. Gaspar, A. Silva, Modelling the degradation and service life of ETICS in external walls, Mater. Struct. 48 (7) (2015) 2235–2249, https://doi.org/10.1617/s11527-014-0305-8.
[50] V. Peixoto De Freitas, A. Costa, and J. M. P. Q. Delgado, "Building Pathology and Rehabilitation Volume 1 Series Editors." [Online]. Available: http://www.springer.com/series/10019.
[51] M. d'Halewyn. *Aspergillus niger*, Compendium sur les moisissures. Institut National de Santé Publique du Québec.
[52] M. d'Halewyn. *Penicillium* spp., Compendium sur les moisissures. Institut National de Santé Publique du Québec.
[53] B. Amaro, D. Saraiva, J. De Brito, I. Flores-Colen, Statistical survey of the pathology, diagnosis and rehabilitation of ETICS in walls, J. Civ. Eng. Manage. 20 (4) (2014) 511–526, https://doi.org/10.3846/13923730.2013.801923. Taylor and Francis.